5-2011

Vascular Smooth Muscle Cells in Response to Gold Nanoparticles

William Mcallister
Clemson University, wmcalli@g.clemson.edu

Vascular Smooth Muscle Cells in Response to Gold Nanoparticles

---

A Thesis
Presented to
The Graduate School of
Clemson University

In Partial Fulfillment
of the Requirements for the Degree
Master of Science
Bioengineering

By
William Bradley McAllister
May 2011

Accepted by:
Dr. Delphine Dean, Committee Chair
Dr. Frank Alexis
Dr. Christopher Kitchens

ABSTRACT

In this master's thesis we look at elucidating the interactions between nanoparticles and cells. Specifically, we looked at how the cell mechanics are affected, cytotoxicity of the nanoparticles, and shifts in cell phenotypes. There has been much research looking into whether nanoparticles are cytotoxic, but limited amounts looking at their effect on mechanics especially with vascular smooth muscle cells. This cell type has two distinct phenotypes of synthetic and contractile that each serve different purposes physiologically.

The first experiments we did were cytotoxicity assays to see if the cells could survive the treatment with nanoparticles. If the cells died within a short period of time then we wouldn't be able to take the next step and look at the mechanics of the cells. Most of the nanoparticles used proved to cause no change in proliferation rate of the cells; however, a couple did show some cytotoxic effects and were not used for further experimentation.

Since the cells were surviving and proliferating after treatment with these nanoparticles we did atomic force microscopy to determine the elastic modulus of the cells that were treated with nanoparticles and those that were untreated. This allowed us to see if there was a significant increase or decrease caused by the nanoparticles. The results showed that there was a significant decrease in the elastic modulus of the cells treated with nanoparticles.

Finally, we wanted to observe any possible phenotypic shifts in the cells by using immunofluorescence. The cells were stained for actin, microtubules (the main components of the cell's cytoskeleton and thus mechanics), and nuclei. Vascular smooth muscle cells at low passage number in culture are typically in the contractile phase and this was proven with our images. The nanoparticle treated cells showed a shift towards the synthetic phenotype which confirmed the decrease in elastic modulus from the AFM data. So, while these nanoparticles are not cytotoxic we are causing a significant change in the cells' mechanics and phenotype.

DEDICATION

This work is dedicated to my parents, Bick and Retta, who instilled in me a constant drive for knowledge and provided me with endless encouragement that I could achieve anything I put my full effort into.

ACKNOWLEDGEMENTS

I would like to thank my advisor, Dr. Delphine Dean who always gave me positive reinforcement no matter the situation and was always willing to help. I would also like to thank my committee members Dr. Christopher Kitchens and Dr. Frank Alexis who have also been extremely helpful with my research throughout. Additionally, I would like to thank Brad Winn and Chaitra Cheluvaraju for their help in learning to isolate vascular smooth muscle cells.

Table of Contents

LIST OF FIGURES

Figure Page

CHAPTER 1

INTRODUCTION TO NANOTECHNOLOGY

Nanotechnology has shown great potential for a wide range of fields, from materials manufacturing to bioimaging[1-3]. Nanoparticles, particles that range from 1-100 nanometers in size (one billionth of a meter), are currently being used for specific biomedical applications like drug delivery to cancer tumors. However, while nanoparticles have shown great promise in these areas, longer term biological effects of nanomaterials are not well-understood. As a cause for concern, some nanomaterials have recently been shown to be able to induce cancer in animal models. Therefore, there is a great need for more thorough investigations on how cells interact with nanomaterials to help elucidate how nanoparticles can affect cellular functions.

Cytotoxicity of Nanoparticles

Cytotoxicity of nanoparticles is a very important factor to look at when talking about how they interact with an organism, since cytotoxic particles lead to increased cell death. Nanoparticles (NPs) in the environment can interact with the respiratory system when inhaled, or they can enter the body via ingestion or injection as well. Mixed results have been attained *in vitro*; some cell types die in response to NP treatment whereas others show very little response. For instance, gold NPs have been shown to cause severe adverse responses in human dermal fibroblasts [4] and Cos-1 cells [5] yet in human leukemic cells [6] and murine macrophages [7], similar particles were internalized by the

cells but caused no further cellular reaction. Clearly there is still some risk involved with these specific gold NPs and further development of this field needs to occur before nanomaterials will be prominent in the clinical setting.

Chen et al. [8] made some interesting discoveries involving gold NPs. Their experimental setup was an *in vivo* study with BALB/C mice that were given varying sizes of gold NPs. The results they found were that the survival of the mice depended on the size of the NPs administered. Mice that were given 3, 5, 50, and 100 nm gold NPs showed no ill effects, but mice that received NP sizes between 8 and 37 nm in most cases died within three weeks. While some NPs may appear to be safe there seems to be other factors involved specific to each NP system.

Nanoparticles for Drug Delivery

Nanoparticles diffuse through blood vessels easily so they can be dispersed systemically very quickly. In addition, nanoparticles can cause very diverse individual cell interactions; they are so small that they can enter cells, organelles, and even DNA easily. As many of the cellular events and processes occur at the nanoscale we may be able to use nanotechnology to assess many of our current techniques faster and more efficiently [9]. This has given us the possibility of novel techniques for cancer drug delivery systems as well as more efficient ways to diagnose and treat diseases. For instance, studies have shown that nanoparticles are able to infiltrate cancerous tumors with a large degree of specificity. [10,11]

Many groups are investigating drug delivery systems at the nanoscale for multiple reasons. Traditional injected and orally administered drugs aren't always the most efficient formulations. The new nanoscale delivery systems are able to give much more precise targeting. Also, this will drive the market to produce better and more efficient drug delivery systems due to competition with current methods.

Nanoparticles for Imaging

Gold nanoparticles modified with antibodies specific to a certain cancer cell protein type are being used in imaging. For example, gold nanoparticles conjugated with antibodies specific for epithelial growth factor receptor were incubated with epithelial cancerous cells as well as non-cancerous epithelial cells. Light microscopy was done to look at the binding affinity and the cancerous cells had six times as many nanoparticle conjugates bound as the non-cancerous cells. This illustrates a potential technique to develop into a means for detecting cancer [12]. Other studies have looked at using similar conjugates in nanorod and nanoshell form with cell specific antibodies for photothermal therapy to heat up cancerous cells and kill them when exposed to infrared light [13-15].

There are movements towards developing multifunctional nanomaterial systems that could identify, visualize, and treat cancer or other diseases [16]. With a single system that could essentially do all of these functions that would be a large advance in the field of cancer treatments. A couple of nanoparticle systems that have gone through clinical trials and are FDA approved for cancer treatment. Abraxan®, which is used to

treat metastatic breast cancer, uses albumin nanoparticles conjugated with taxol. Doxil® is used to treat ovarian carcinoma using a liposome system that carries doxorubicin to treat the cancer.

There is also the ability to label cells using certain NP systems that would allow for specific cells to be monitored over a long period of time rather than at one specific instance. Schweiger et al. [17] have developed a preliminary system using poly(ethylene imine)-g-poly(ethylene glycol) with iron oxide NPs to demonstrate this technique. Their results have shown that they can create a stable NP environment where the NPs stay suspended in cell media and cause little to no cytotoxicity. The hydrophilic PEG group located in the backbone of the polymer structure is believed to be the reason for low cytotoxicity. These properties indicate that this system would be useful for cell tracking intentions.

Green Synthesis Techniques

There has been a push recently to develop a better way to produce NPs because some of the toxicity reports found can be traced back to the ingredients used to synthesize the NP systems. Therefore, a green initiative is being pursued to help prevent this issue. Das et al. [18] have demonstrated a technique to create Gold NPs using ethanolic flower extract (EFE) from *Nyctanthes arbortristis* as the reducing agent during the synthesis of these Gold NPs. Their results showed the NPs were well capped which is necessary for many biomedical applications to shield the metal core from an *in vivo* environment.

Leonard et al. [19] also were able to successfully produce gold NPs without the use of the conventional reducing agent. Korean red ginseng root (Panx ginseng) was used without any additional capping reagents to generate the gold NPs. Their results showed the NP system did not aggregate meaning that the phytochemicals from the ginseng provided a great coating of the NPs. They were also able to produce favorable size distributions during the synthesis process and cytotoxicity tests showed very few cells *in vitro* were killed by the gold NPs. While these green techniques are relatively new they do show great promise to giving the next step for use in biomedical applications without the use of toxic solvents in preparation of the NPs.

Nanoparticles for Tissue Engineering

The potential to initiate stem cell differentiation is a fascinating idea that one could obtain a specific cell type simply by delivering nanoparticles through the cell membrane. A specific study has looked at the use of citrate capped gold nanoparticles to induce differentiation of mesenchymal stem cells. They were able to promote osteogenic differentiation while inhibiting adipogenic differentiation. This was done by activating the p38 MAPK pathway, which was accomplished by the nanoparticles interrupting certain cellular signaling pathways [20-23]. This served as a stress inducer on the cell that activated the MAPK signaling pathway that causes the upregulation of osteogenic genes.

Lin et al. [24] developed a technique of labeling stem cells and acinar cells with NPs as a technique to help replace salivary gland cells damaged during radiotherapy

treatment in the head and neck region. Their results showed that with a co-culture system of these two cell types, they could differentiate the bone marrow stem cells into acinar like cells and begin to regenerate the salivary glands; however, acinar cells by themselves had a better therapeutic effect. The NPs were used to identify where the cells were going after they were injected.

Another interesting topic for NPs is utilizing biodegradable systems where there aren't any foreign substances left in the body. Wang et al. [25] showed the ability to create a novel colloidal gel using PLGA NPs that were oppositely charged with chitosan and alginate to create a construct on the macroscale (2mmx2mmx1mm scaffold). Due to the opposite charge of the NPs in the gel a cohesive strength was created. Their testing of the material showed that it could be suitable for tissue engineering applications; it is not cytotoxic and has proven mechanical properties, while also allowing for extended release of growth factors and other active ingredients during its degradation. The ability of a material to degrade in the body to non-toxic substances could eliminate the need for constant evaluation of other NP systems.

Magnetic Nanoparticles

Magnetic NPs introduce a unique strategy for treating cancer types, as they can be modified to target specific receptors upregulated in cancerous tumors and when introduced to a magnetic field the NP vibrations will cause an increase in temperature. This increase in cell temperature can trigger apoptosis allowing for a specific and safe treatment called hyperthermia. Elsherbini et al [26] demonstrated this using

superparamagnetic iron oxide NPs (Fe_3O_4) targeted to Ehrlich tumors which is a type of carcinoma. Their results showed they were able to heat the tumor region to temperatures that caused apoptosis of the carcinoma cells and significantly reduce the size of the tumors *in vivo*.

Another study conducted by Liu et al. [27] was done looking at the biocompatibility of Fe3O4 NPs at different concentrations amongst several different cell lines. Multiple assays were conducted to look at cell viability, apoptosis, oxidative stress, and the cell cycle. TEM was also done to visualize the particles to show cellular uptake. The results from this study showed that they were capable of efficiently labeling the individual cells but were not harmful the cells examined.

There are also groups working on combinations of these subsets in nanoscience. Hsieh et al. [28] demonstrated a way to create magnetite NPs for hyperthermia treatments using a green fabrication technique as some other magnetite NPs have been shown to aggregate and have biocompatibility issues. This group has reported a new method of fabrication of magnetite NPs using a co-precipitation technique within the pores of agar gel. These newly made gels were dried under vacuum and ground into powder leaving agar-conjugated magnetite NPs. The particles were analyzed with TEM, FTIR, and XRD among others to characterize the particle type. Cell viability assays were done using the NPs and showed that the cells were proliferating more than the controls, meaning that these NPs are safe and can be considered for more therapeutic applications.

The illustration seen below shows the reaction used to obtain the gold NPs that we used for our studies.

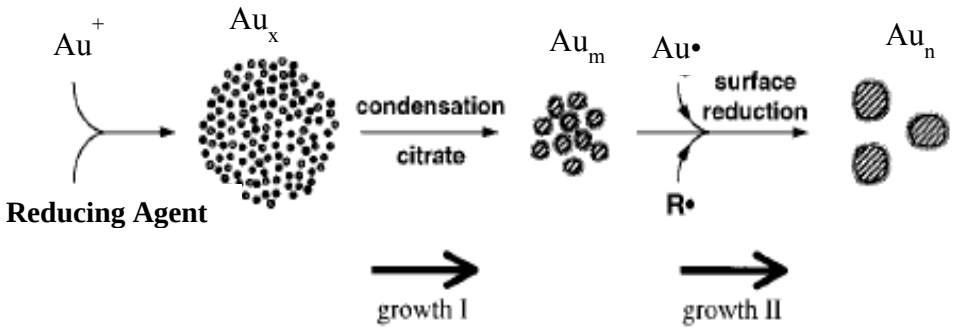

Modified from *J. Phys. Chem. B.* **1999**, 103, 9533-9539

Figure 1.1. The steps used to obtain capped gold NPs with citrate.

In Figure 2.2 below you can see what the gold NPs we used would look like on a macroscale.

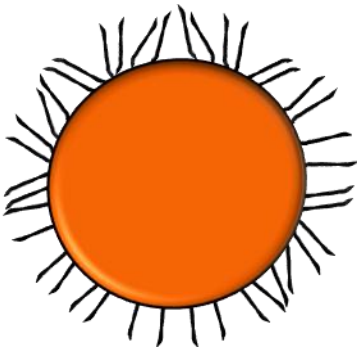

Figure 1.2. Au NP on the macroscale

In conclusion, there are really limitless possibilities for where nanoscience is going and what it will ultimately be able to do. The effect on the environment is important which is why so many groups are working diligently to overcome these issues. While there are still many humps to get over before they are considered safe as well as effective, once the field has reached that point the possibilities will be endless. This field will continue to emerge and develop for years to come and will eventually become part of everyday treatments.

CHAPTER 2

VASCULAR SMOOTH MUSCLE CELLS AND THEIR SIGNIFICANCE

Vascular smooth muscle cells (VSMC) are found throughout the body in the tunica media of the arteries and veins in the cardiovascular system. As the tunica media is the layer responsible for regulating lumen size in the arteries and veins, the primary function of VSMCs is contraction [29]. The VSMC cytoskeleton has several components that give it the cell its usual contractile phenotype. Actin filaments are thought to be the primary structural component of most cells, are stiff, quickly respond to external forces, and are important in cell migration [30]. Microtubules are another component of the cytoskeleton. They have a larger diameter than actin filaments and a higher bending stiffness than actin due to their tubular structure. A third component of the cytoskeleton is intermediate filaments, which are highly dynamic as are the other cytoskeleton components [31].

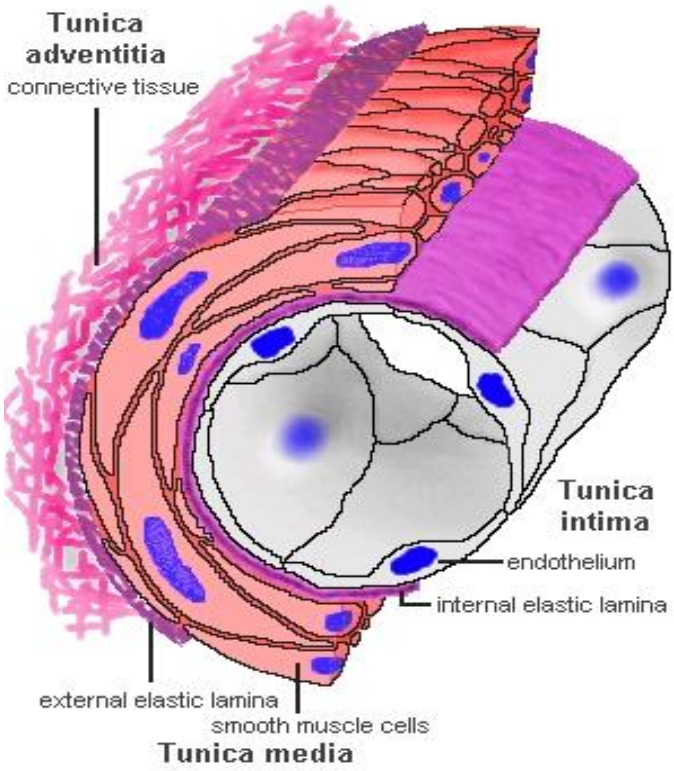

www.lab.anhb.uwa.edu.au

Figure 2.1. A schematic of an artery showing where the vascular smooth muscle cells are present.

Vascular smooth muscle cells (VSMCs) are useful in research because they have two specific phenotypes for the function they will be performing within an artery in the body. The location of VSMCs can be seen in Figure 3.1 above. The contractile phenotype has more contractile, functional actin filaments inside the cell. The synthetic phenotype has more organelles in the cytoplasm, which are mostly involved in protein synthesis and therefore are more proliferative than the contractile type. There are

morphological differences between the two as the contractile type is more elongated and spindle-like while the synthetic time is less elongated and more spherical. In addition, there are a couple other methods to determine which cell type is present.

The first option is looking at specific marker proteins being upregulated in the cells: alpha-smooth muscle actin, smooth muscle-heavy chain myosin, smoothelin-A/B, SMemb/non-muscle MHC isoform-B and cellular retinol binding protein. Some of these marker proteins are used in cellular contraction and therefore only present in the contractile cell type while others are upregulated in proliferating, synthetic cells [32,33]. As the cells are held in culture longer the amount of expression of these contractile markers decreases and more cells will become synthetic [34]. Due to varying levels of expression from these proteins at least two of the contractile markers need to be upregulated in order to label a cell as contractile (alpha-smooth muscle actin, smooth muscle-myosin heavy chain, and smoothelin are specific to contractile cells). A newer alternate technique that can be used is atomic force microscopy (AFM). AFM can be used to measure the elastic modulus of the cells. Contractile cells have a much higher modulus as the actin is more organized inside the cell making it stiffer than synthetic cells.

Vascular smooth muscle cells perform several roles in an arterial wall and they play a significant role in the pathenogenesis of atherosclerosis. In 2006, it was estimated that approximately 17.6 million people in the USA have severe atherosclerosis caused by the narrowing of the coronary arteries due to plaque buildup

(http://www.americanheart.org/presenter.jhtml?identifier=4478). As seen in Figure 3.2 below, the plaque buildup can significantly decrease the amount of blood flow through arteries to certain parts of the body. Some of the most common places for plaque to build up are in the coronary arteries around the heart which can cause a heart attack and buildup in the carotid arteries that deliver blood to the brain and can cause a stroke.

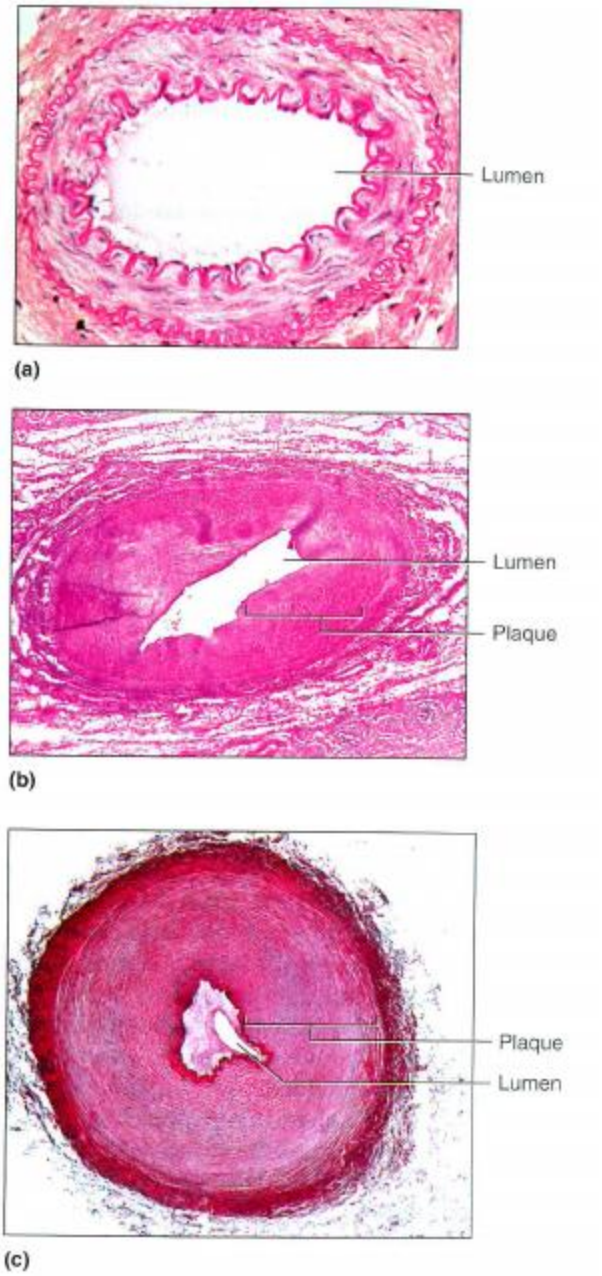

Figure 2.2. Development and Progression of Atherosclerosis (a) healthy artery (b) plaque development in artery and (c) severe occlusion of artery. [35]

When an injury occurs the cells in the area tend to de-differentiate towards the synthetic phenotype. This increase in synthetic cell type as well as cell number is in part

what leads to the development of atherosclerosis. This de-differentiation occurs due to exposure to certain growth factors and inflammatory mediators that macrophages release due to contact with low density lipoproteins. These cells will then move toward the subintimal space and help develop a fibrous cap on top of the atherosclerotic plaque. Collagen synthesis is then promoted by interferon that is released by macrophages which will help to alleviate stress on the fibrous cap. However, matrix metalloproteinases can be released from macrophages and synthetic vascular smooth muscle cells and cause thrombus formation [36].

Since vascular smooth muscle cells that are in culture longer trend towards the synthetic type like that found in atherosclerosis we will use high passage cells as well as low passage cells for our experiments. It is still very unclear as to what the mechanism is that causes the dedifferentiation of cells from contractile to synthetic, and this shift is something that needs to be clearly understood at which time treatments can be tailored specifically to differentiate cells back into the contractile type. Until that is defined our studies are focused on the effects of NPs are healthy VSMCs.

The overarching goal of this study is to analyze the mechanical and structural effects that metallic, specifically gold, NPs have on VSMCs. A comprehensive look into these parameters will help devise a new strategy in the nanotechnology world, as we cannot simply be concerned if nanomaterials are immediately toxic to cells. A change in structure and function of a cell could ultimately lead to other problems over a longer period of time, which is one of the main considerations of this project.

CHAPTER 3

VASCULAR SMOOTH MUSCLE CELL MECHANICS IN RESPONSE TO GOLD NANOPARTICLES

Abstract

Nanotechnology has shown great potential toward biomedical engineering for applications in bioimaging to tissue engineering. However, while there has been possible great promise seen in these areas longer term biological effects of nanomaterials are not well-understood. In the current study, the mechanical, phenotypic, and cytotoxicity properties were assessed using vascular smooth muscle cells treated with various nanoparticle systems. The mechanical properties of the rat aortic VSMCs were evaluated using atomic force microscopy and a standard cytotoxicity assay was performed as well as immunostaining to look at the cytoskeletal elements. Results show the cells are surviving most nanoparticle systems; however the elastic modulus of the cells is significantly reduced. Immunostaining indicates that a phenotypic shift may be occurring from a contractile state to a synthetic state after treatment with nanoparticles. So, while the particles aren't toxic to the cells they are still causing a significant change in the cell mechanics.

Introduction

Nanotechnology has shown great potential toward biomedical engineering for applications in drug delivery to bioimaging to tissue engineering[1-3]. Nanoparticles are

interesting to look at in reference to individual cell interactions as they are so small that they can enter cells, organelles, and even DNA easily. As many of the cellular events and processes occur at the nanoscale we may be able to use nanotechnology to assess many of our current techniques faster and more efficiently [4]. There are new approaches being used for site-specific drug delivery using nanoparticle systems and studies have shown that nanoparticles are able to infiltrate cancerous tumors with a large degree of specificity [5,6]. Gold nanoparticles can be conjugated with antibodies specific to certain receptors that are upregulated in certain cancer types. This allows for the cancerous cells to bind significantly more NPs which can be seen using different detection techniques [7]. NPs have also been used to help induce differentiation of stem cells for tissue engineering applications. Citrate capped gold NPs given to mesenchymal stem cells have been shown to induce a shift toward osteogenic differentiation while inhibiting adipogenic differentiation. This was done by activating the p38 MAPK pathway, which was accomplished by the nanoparticles interrupting certain cellular signaling pathways [20-23].

However, while NPs have shown great promise in these areas, longer term biological effects of nanomaterials are not well-understood and there is still concern as to whether or not NPs can be used as safe therapeutic agents. As a cause for concern, some nanomaterials have recently been shown to induce cancer in animal models. Therefore, there is a great need for more thorough investigations on nanomaterials and cell interactions to help elucidate how nanoparticles can affect cell function.

Vascular smooth muscle cells are found throughout the body in the tunica media of the arteries and veins in the cardiovascular system. As the tunica media is the layer responsible for regulating lumen size in the arteries and veins, the primary function of VSMCs is contraction [29]. The VSMC cytoskeleton has several components that give it the cell its usual contractile phenotype. Actin filaments are thought to be the primary structural component of most cells, are stiff, quickly respond to external forces, and are important in cell migration [30]. Microtubules are another component of the cytoskeleton. They have a larger diameter than actin filaments and a higher bending stiffness than actin due to their tubular structure. A third component of the cytoskeleton is intermediate filaments, which are highly dynamic as are the other cytoskeleton components [31].

The goal of this study was to determine any structural or mechanical changes in VSMCs when treated with metallic NPs.

Materials and Methods

Cell Culture

Rat aortic VSMCs were isolated from adult Sprague Dawley rats and cultured in Dulbecco's Modified Eagle's Medium (DMEM) (Fisher Scientific) with 10 % fetal bovine serum (FBS) (Sigma) and 1% antibiotic-antimycotic solution (Sigma). VSMCs were maintained in polystyrene T-75 flasks in an incubator at 37°C and 5% CO2. The cell media was replaced every 48 hours with fresh media. Cells were used between passage 5 and 8 for low passage experiments and between 10 and 13 for high passage

experiments. They were grown to approximately 80% confluency in flasks when they were trypsinized with 0.25% trypsin with 0.02% ethyldiaminetetaacetic acid (Sigma). The cells were seeded at a density of 30,000 cells/cm^2 on 22x22 mm coverslips coated in 1 mg/ml rat tail type I collagen (BD Sciences) 24 hours prior to seeding the cells [37]. The coverslips were kept in 6 well plates in the incubator at 37°C and 5% CO2. The cells weren't seeded confluently so that there was no overlapping occurring, which is known to change the stiffness properties of the cells in a confluent environment. There were three groups of cells for low passage and high passage experiments: untreated cells, control solution treated cells, and NP treated cells. The control solution consisted of the solution used to cap the NPs without any NPs present. Untreated cells were given PBS. The cells were treated 2 days prior to AFM testing.

Nanoparticle Synthesis

The metal precursor hydrogen tetrachloroaurate (III) trihydrate ($HAuCl_4 \cdot 3H_2O$, 99.99%), stabilizing agent sodium citrate dihydrate (99%, part no. BDH0288), and reducing agent sodium borohydride (98%) were purchased from VWR. The stabilizing agents carboxy methyl cellulose (CMC, MW = 90,000), Pluronic F-127, and Pluronic F-68 were purchased from Sigma-Aldrich. All chemicals were used without further purification.

It should be noted that the Pluronic F-127 capped NPs killed all cells as seen in the light miscroscopy images below within 48 hours of treatment and was therefore not used for any further experiments.

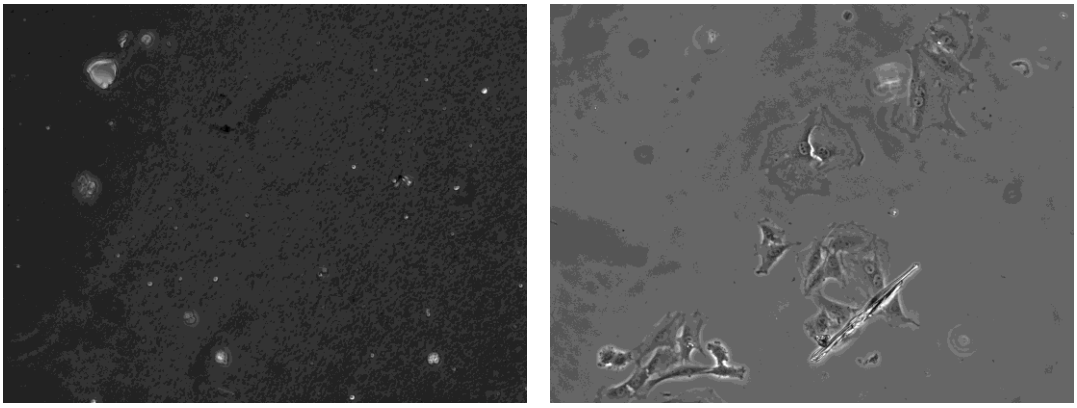

Figure 3.1. Light microscopy images of NPs coated with pluronic F-127 (left) treated cells and cells treated with just the pluronic F-127 control solution (right). The NP treated cells all died within 48 hours of treatment.

Characterization

Transmission Electron Microscopy (TEM)

All TEM images were obtained using a Hitachi 7600 with a 120 kV accelerating voltage. TEM samples were prepared either by gentle aspiration or drop casting (~5 μL) of the nanoparticle dispersion onto a 300 mesh formvar carbon coated copper TEM grid (Ted Pella), followed by solvent evaporation. The size distributions were obtained by image analysis performed with the ImageJ software package[1] counting at least 300 particles for meaningful and relevant statistics.

Ultraviolet-visible (UV-VIS) *spectroscopy*

UV-VIS characterization was performed on a Varian Cary 50 spectrophotometer. All samples were measured in a 1 cm path length quartz cuvette during UV-VIS measurements. Deionized water was used for background correction of all UV-VIS spectra.

Gold Nanoparticle Synthesis

Citrate stabilized gold nanoparticles (GNPs) were prepared by a modified procedure similar to Jana et al.[2] yielding ~4 nm diameter particles. In short, 100 μL of citrate solution (0.05 M) and 100 μL of $HAuCl_4$ (0.05M) were diluted to 20 mL with deionized water. The aqueous gold/citrate mixture was reduced by the addition of 100 μL of $NaBH_4$ (0.05 M) which yielded a ruby red GNP dispersion. CMC stabilized GNPs were prepared by adding 100 μL $HAuCl_4$ (0.05 M) to a 0.1wt% CMC solution, followed by subsequent reduction with 100 μL of $NaBH_4$ (0.05 M). Pluronic (F-127 or F-68) stabilized GNPs were prepared by adding 100 μL of $HAuCl_4$ (0.05 M) to a 0.1wt% solution of Pluronic solution in deionized water. The gold ions were reduced with 600 μL $NaBH_4$ (0.05 M) creating a red/purple colored GNP dispersion.

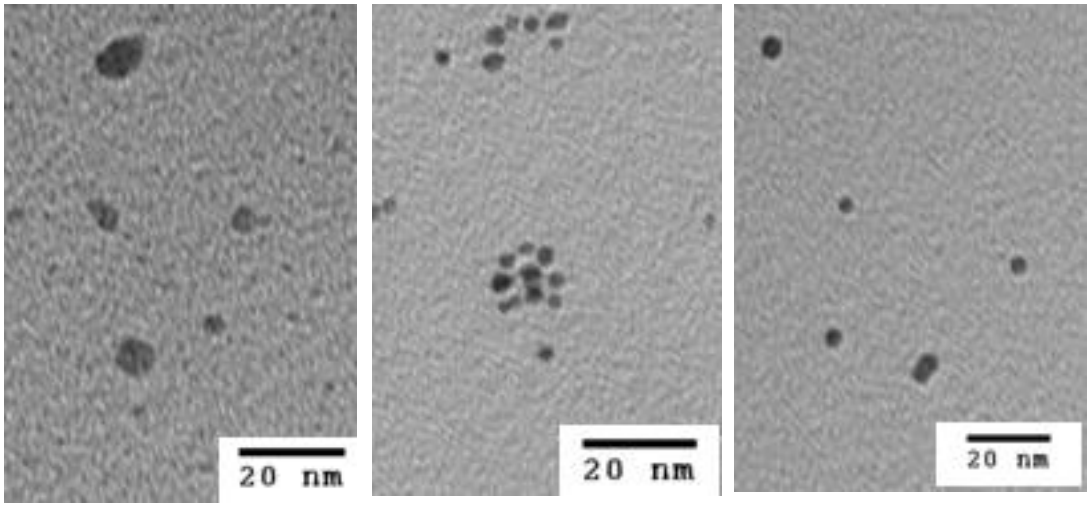

Figure 3.2. TEM images of each different NP system used in our study.

AFM Testing

The AFM testing was done 2 days after cell treatments. The high passage experiments were done on a Veeco Dimension (3100?) and the low passage experiments were done on an Asylum Research MFP3D, and they were both operated in contact mode in fluid. Testing was done while cells were still on the coverslips and media was exchanged for warm media every 30 minutes. Cells were chosen at random during experimentation (n=10). The AFM probe used was a borosilicate spherical tip with a 5um diameter and a 0.12 N/m spring constant. The probe was centered over the cell prior to indentation.

Each cell indentation was approximately 500 nm and we applied the Hertz Model to approximately the first 150 nm of each indentation.

Force Curve Analysis

A series of MATLAB scripts were implemented to analyze the data collected from the AFM. The script converted a text files to matrices with displacement, and the respective deflection for the extension and retraction of the tip.

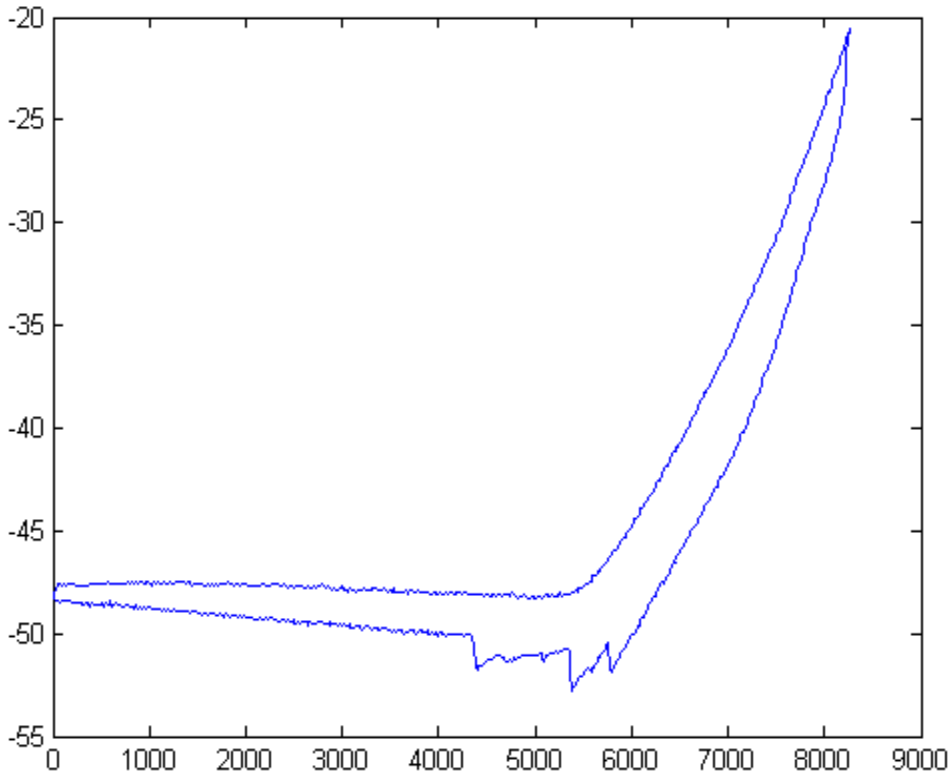

Figure 3.3. Plot of extension and retraction raw data.

The contact point was selected for the dataset at the displacement value where the deflection rapidly begins to increase, indicating contact between the cell and the AFM tip. This adjustment allows displacement to represent true indentation. The bias and offset for the deflection was adjusted. The region before the contact point was to have a constant deflection of zero. In order to do this the inner two quartiles of the region between the starting point to the contact point was analyzed. The slope for the inner two quartiles was found using the sum of least squares. The entire dataset was multiplied by the inverse of the slope in order to account for the bias of the AFM. Then the value of the center of this region was subtracted from the entire dataset to account for the offset of the deflection readings. The readings for extension and retraction were adjusted separately due to considerable differences in their biases. The deflection was then multiplied by the spring constant ($k = 0.1416$ N/m) to find the force associated with the indentation.

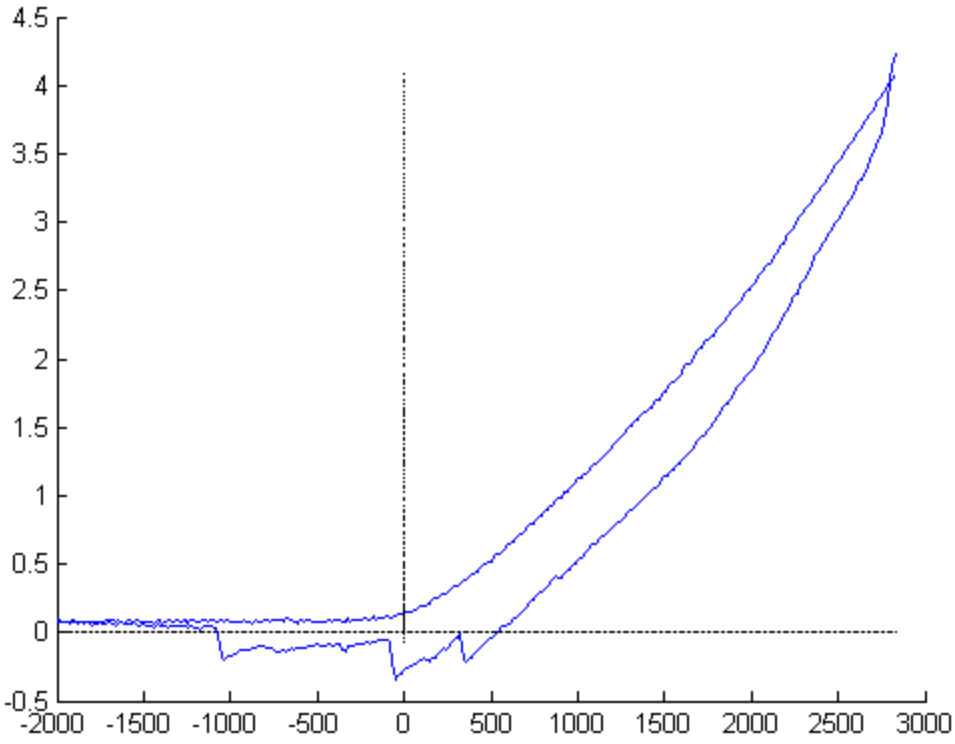

Figure 3.4: Plot of indentation and Force for extension and retraction after adjustments (Force Curve).

The Matlab script continued analysis by finding the elastic modulus by applying the Hertz Model (Fig 4.5) to a selected indentation range.

$$F = \frac{4}{3}\frac{E}{(1-v^{2)}}R^{\frac{1}{2}}\delta^{\frac{3}{2}}$$ Fig 3.5

F and δ represent measured force and indentation depth respectively. R and v are constants for tip radius and Poisson's Ratio respectively. E is the variable of interest representing elasticity. The radius R was set at 2.5μm. For this dataset the values for

elasticity were found for every indentation depth from 100nm to 700nm and averaged an elasticity reading for the force curve.

Cytotoxicity Assay

Cells were placed in 96-well plate at 10,000 cells per well. NP and control solutions as well as equal amount of PBS for were added to each well. Samples were all done in triplicate. After the 2 day treatment period the lysis solution (LS) was added at a ratio of 15 ul LS per 100ul media then incubated for 60 minutes at 37°C. Then transferred 50 ul of the supernatant to enzymatic assay 96 well plate where the 50ul of the reconstituted Substrate Mix was added to each well. The plate was covered and incubated at room temperature for 30 minutes. Then 50 ul of the Stop Solution was added to each well and absorbance readings were taken at 490 nm.

Immunofluorescence Staining

Immunofluorescence staining was done to look at smooth muscle alpha-actin, which is a main protein found in VSMCs, to help visualize phenotypic changes after NP treatment. Cells were fixed with 4% paraformaldehyde for exactly 10 minutes. The cells were then permeabilized with a solution of PBS/0.01M Glycine/0.1% Triton-X (Sigma) for 30 minutes. Then the cells were incubated in blocking solutions with 5% Bovine Serum Albumin (BSA)/PBS for 15 minutes and 5% Normal Serum in 1% BSA/PBS for 15 minutes. Then cells were incubated with rat smooth muscle α-actin monoclonal antibody (COMPANY) overnight at 4°C. This was followed by rinsing and the addition of Rhodamine (TRITC)-conjugated AffiniPure Donkey Anti-mouse IgG (Invitrogen) as a

secondary antibody for 2 hours. Then as the slides were being mounted SlowFade Gold antifade reagent with DAPI was used (Invitrogen).

Statistics

Student's *t* tests were performed on the data sets comparing control cells with control solution treated cells as well as comparing control cells with NP treated cells with an alpha of 0.05 used for each test.

Results

Elastic Modulus

Low passage results

Citrate experiments done on low passage (between 5 and 8) VSMCs have shown that both the control solutions and NPs cause significant decrease in elastic modulus as compared to control cells. The control cells had an elastic modulus of 13.49 ± 1.99 kPa while the control solution treated cells elastic modulus was 4.33±1.51 kPa and the citrate NP treated cells had an elastic modulus of 7.43±4.89 kPa. The CMC data showed a similar trend in that the elastic modulus of both the control solution and the NP solution were significantly lower than the normal VSMCs. The modulus of the control solution cells was 6.86 ± 2.71 kPa and the modulus of the CMC NP treated cells was 7.31 ± 2.23 kPa. All of the experimental groups had a significantly lower modulus ($p<0.05$) than the control untreated VSMCs.

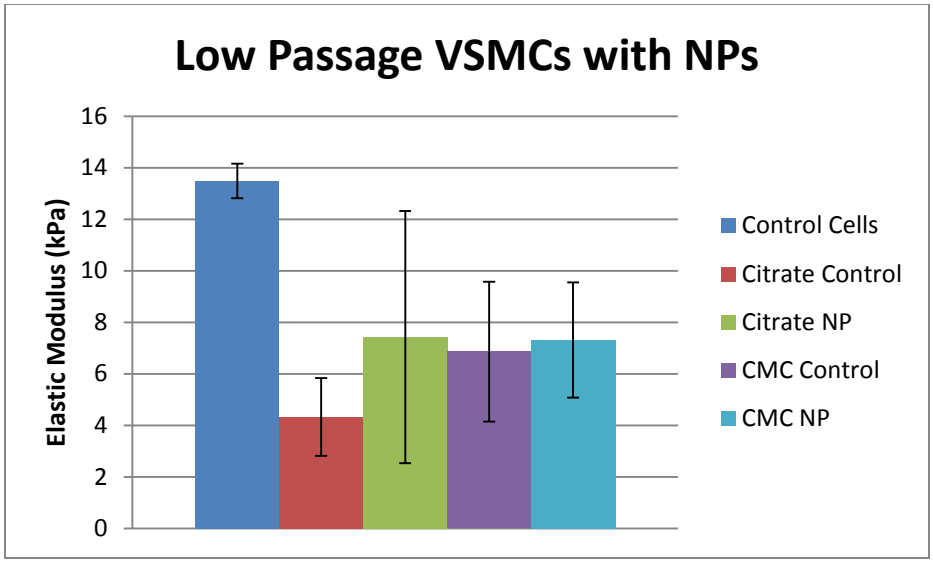

Figure 3.6. The results for the low passage AFM experiments show a significant difference between each treatment as compared to the control cells.

High passage results

Pluronic F-68 NP and control solutions were the only treatment done on high passage VSMCs. These results showed a different than the low passage cells. The control solution treated cells had an elastic modulus of 1.59±0.46 kPa which was significantly lower than the pluronic NP treated cells which had an elastic modulus 7.57±2.19 kPa.

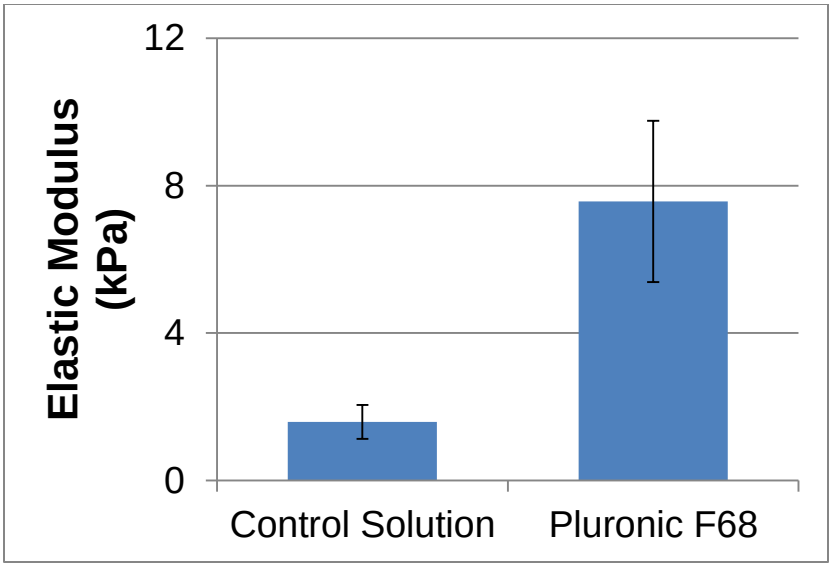

Figure 3.7. Elastic Modulus values of VSMCs after treatment with pluronic F-68 control solution as well as pluronic F-68 capped gold NPs. The NP treated cells had a significantly higher elastic modulus than the control solution treated cells.

Cytotoxicity

Low passage results

Cytotoxicity testing showed that CMC NP treated cells survived 104.6%±16.9 as often as untreated VSMCs and the CMC control solution treated cells survived 94.1%±16.0 as often as the control untreated cells. The citrate experiments showed a similar result in that the citrate NP treated cells survived 118.2±±9.1 as often as the control cells and the citrate control solution treated cells survived 95.4%±21.5 as often as the control VSMCs treated with PBS. Statistics showed no significant difference between the control and the experimental groups.

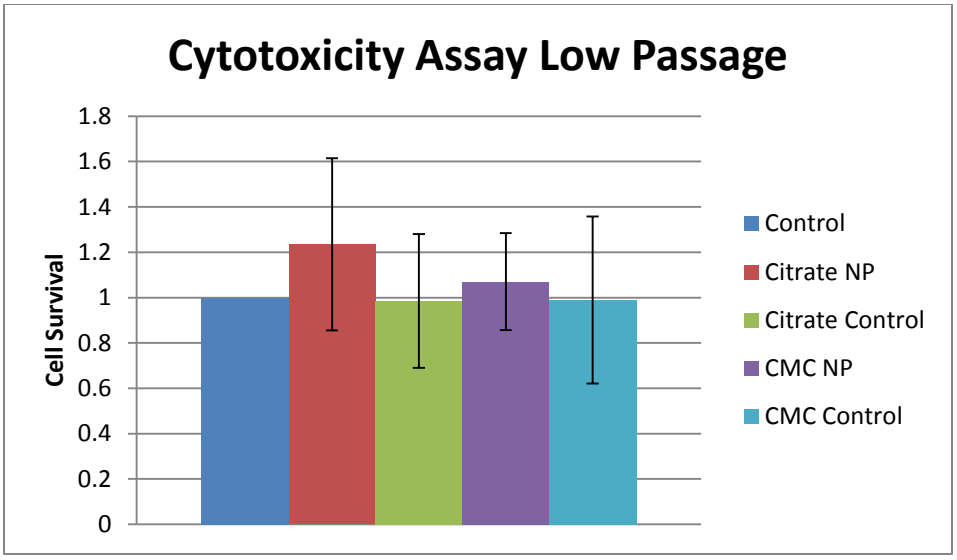

Figure 3.8. Cytotoxicity assay results on low passage VSMCs treated with gold NPs

High passage results

Cytotoxicity results showed that CMC NP treated cells survived 113.5%±55.8 as often as control untreated cells and the control solution treated cells survived 90.7%±2.2 as often as the control untreated cells. The citrate results were similar and showed that citrate NP treated cells survived 96.4%±8.1 as compared to the control cells and the citrate control solution treated cells survived 98.1%±10.3 as often as the control cells. Statistics showed no significant difference between the control and the experimental groups.

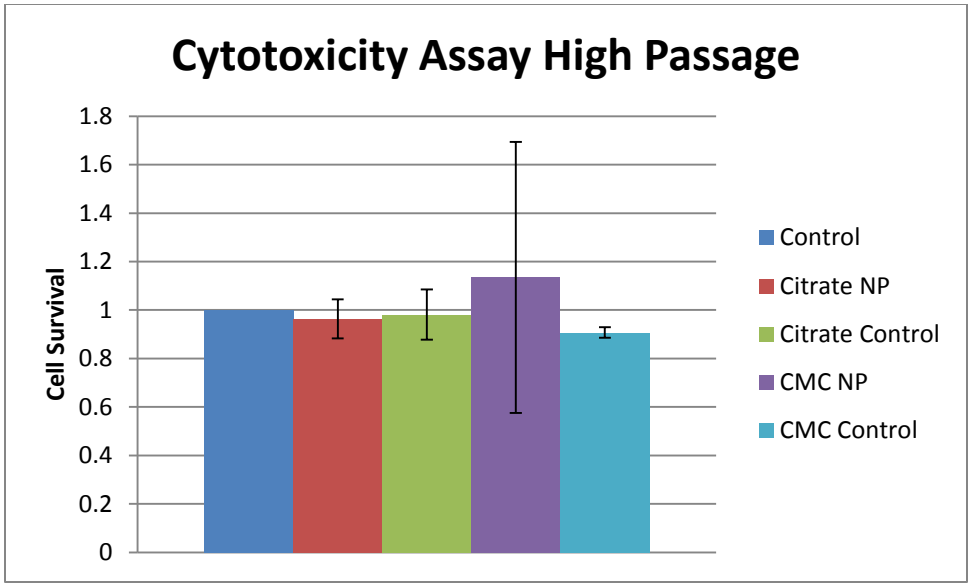

Figure 3.9. Cytotoxicity assay results on high passage VSMCs treated with gold NPs

Immunofluorescence Staining

Low passage results

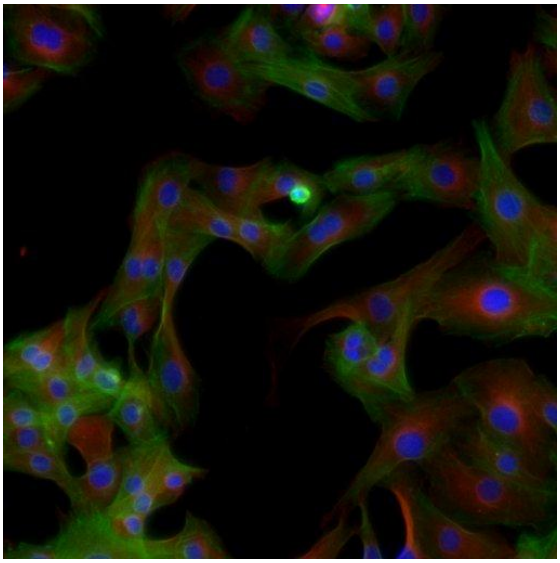

Figure 3.10. Control untreated VSMCs

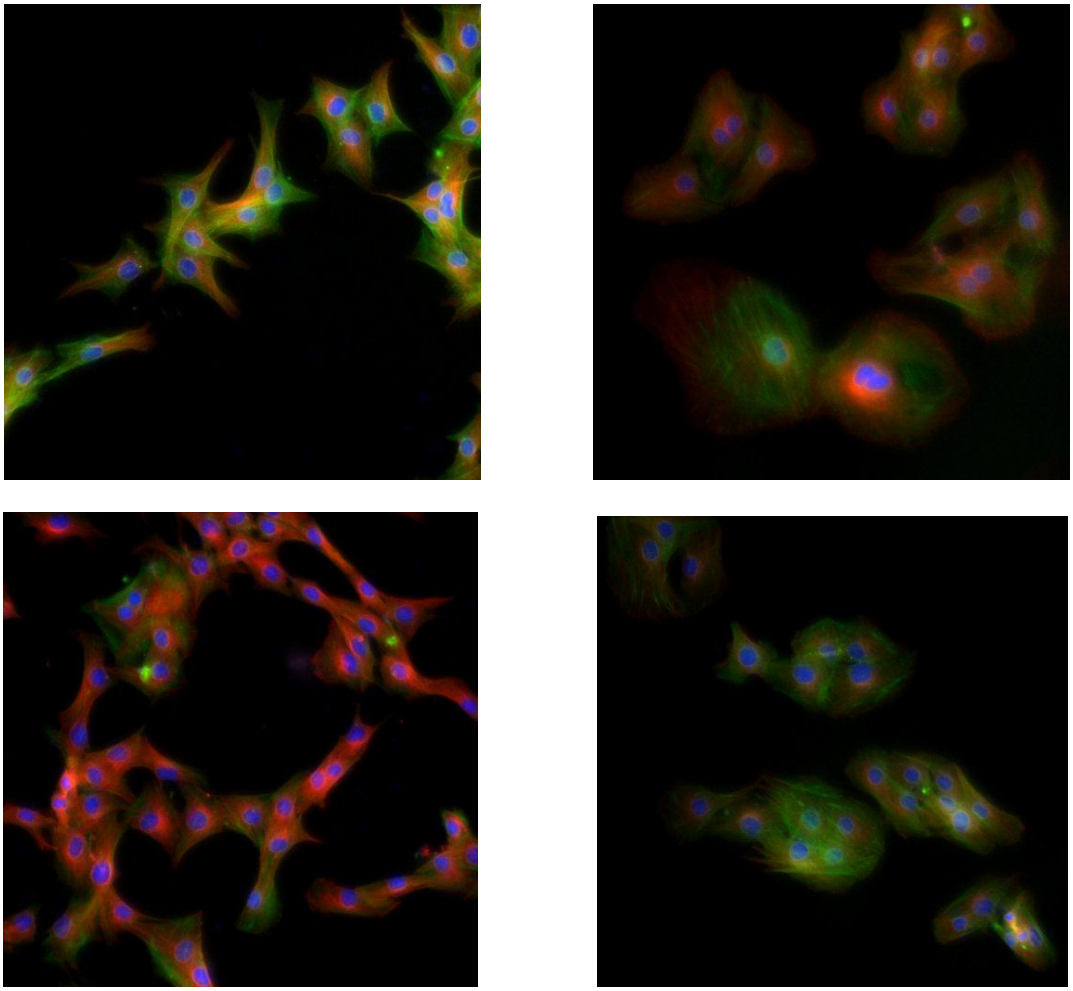

Figure 3.11. Left column is VSMCs treated with sodium citrate Au NPs and the right column is cells treated with sodium citrate control solution

The low passage control cells appear to be more elongated and contractile looking which coincides with the AFM data acquired. The citrate control solution treated cells are much shorter and fatter than the control cells, meaning they are likely in the synthetic phase. However, the images of the citrate NP treated cells appears that they are somewhere in between. Some of the cells look more elongated while others appear more round.

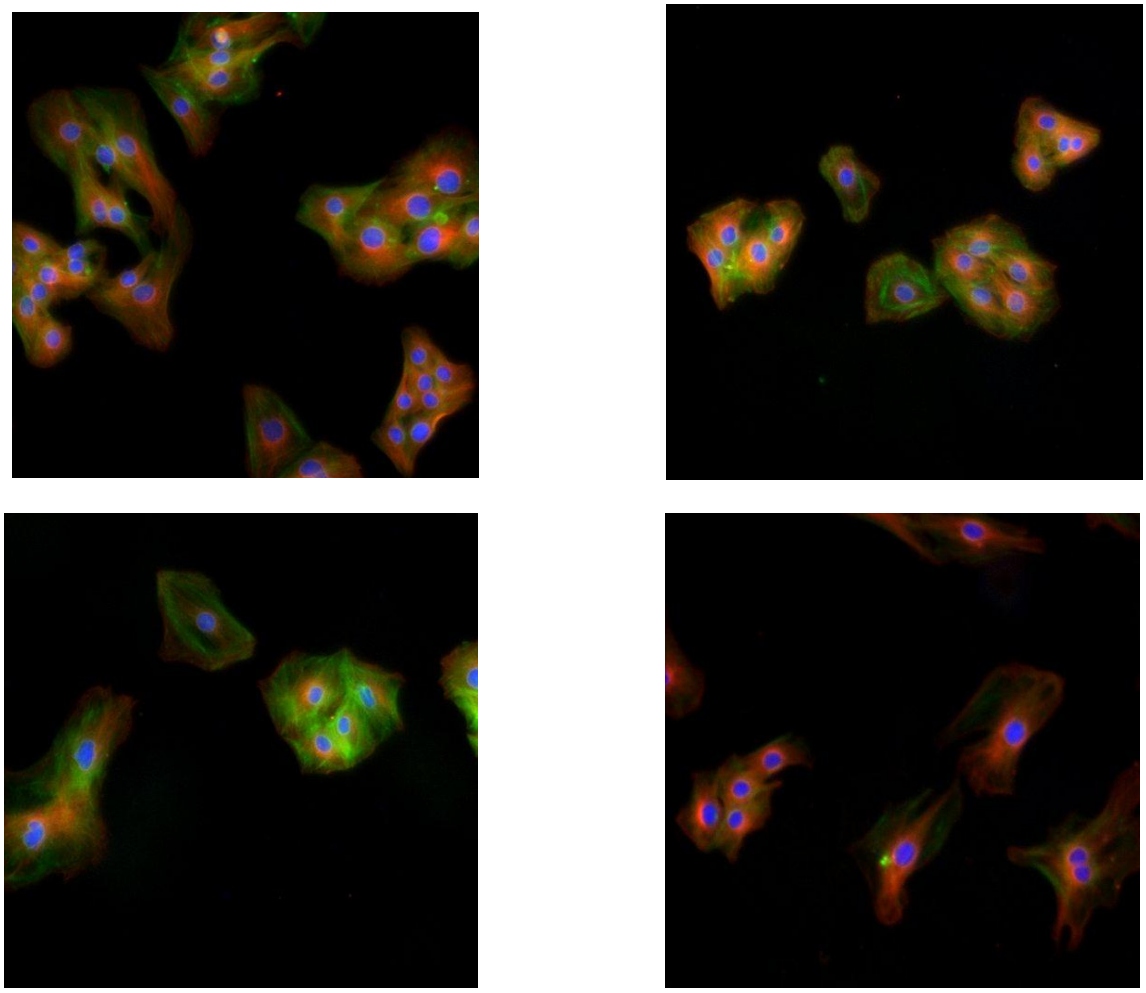

3.12. The left column shows VSMCs treated with CMC capped Au NPs and the right column shows cells treated with CMC control solution

The CMC results show that most of the cells are shorter and rounder compared to the control VSMCs meaning they have all likely shifted to a more synthetic phase.

High passage results

Fluorescence imaging on the high passage cells showed shorter and fatter cells treated with the CMC control solutions while the NP treated cells were more elongated and spindle-like. The citrate solutions gave the opposite effect and showed NP treated cells to be more synthetic while the control solution treated cells seemed more contractile.

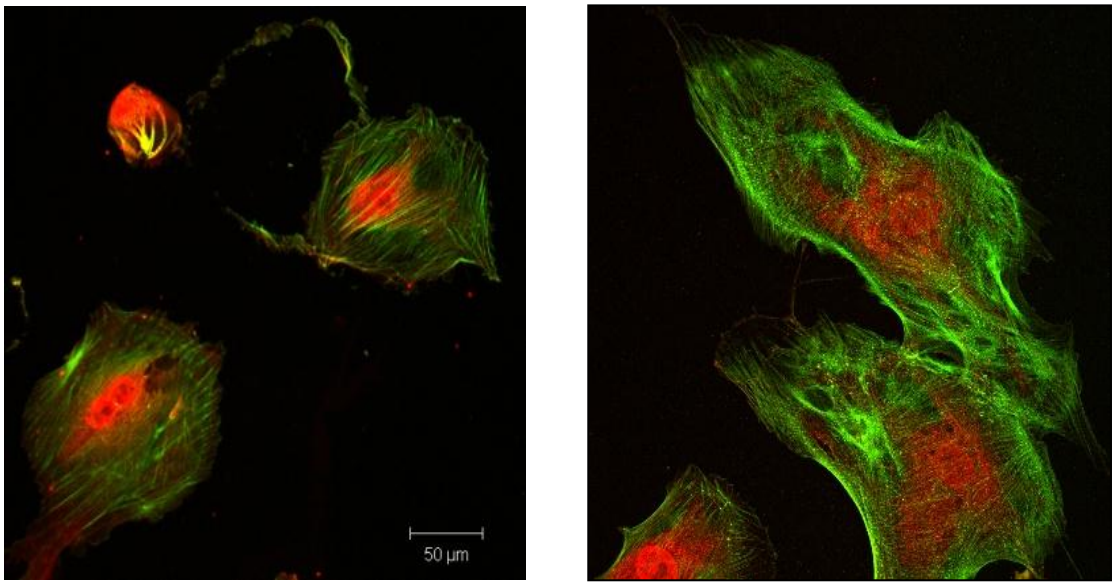

Figure 3.13. Confocal images of VSMCs treated with pluronic F-68 control solution (left) and VSMCs treated with pluronic F-68 capped Au NPs (right)

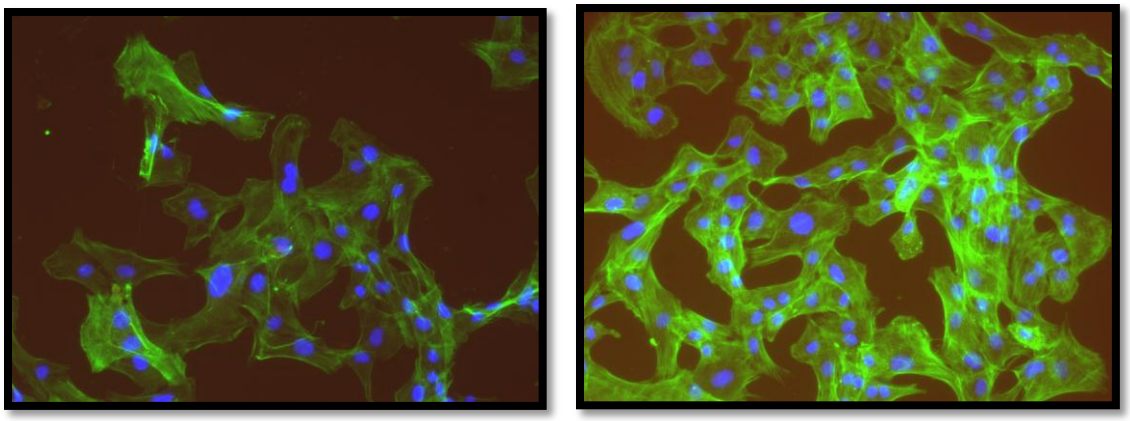

Figure 3.14. Fluorescence images of sodium citrate Au NP treated cells (left) and sodium citrate control treated cells (right)

Citrate control solution treated cells are thicker and more substantial than the cells treated with the capped NPs.

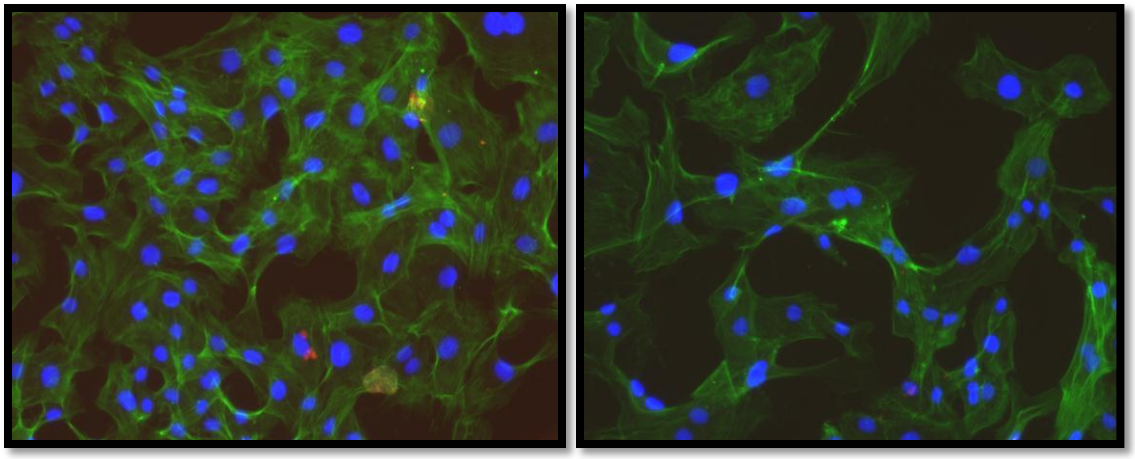

Figure 3.15. CMC Pt NPs (left) and CMC control solution treated cells (right)

VSMCs treated with CMC NPs appear to be more substantial and thicker than the control counterpart.

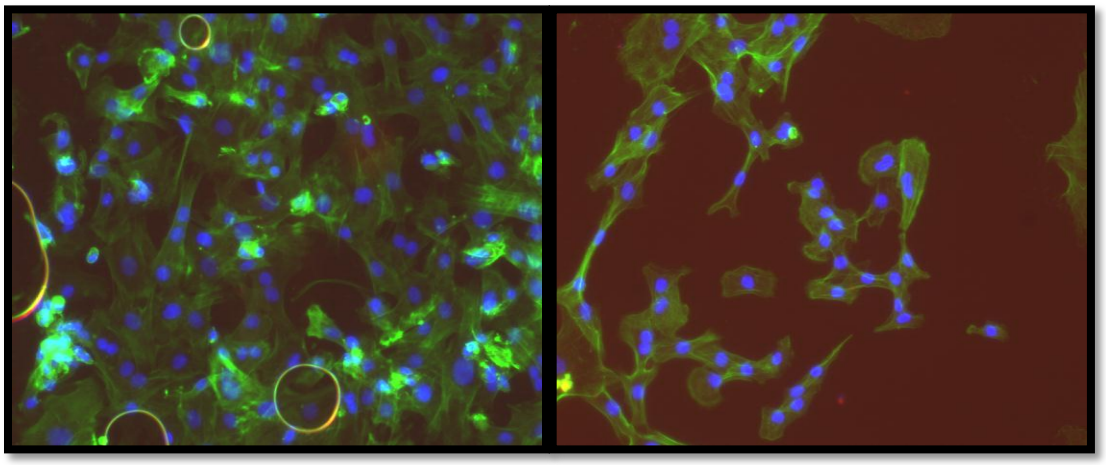

Figure 3.16. 0.1% pluronic F-68 Pt NP's (left) and control solution (right)

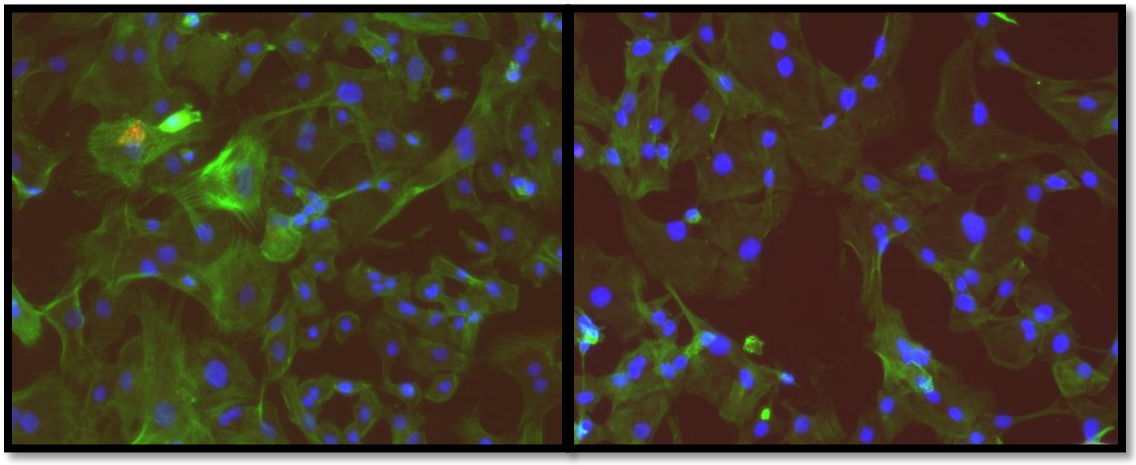

Figure 3.17. 0.15% pluronic F-68 Au NPs (left) and control solution (right)

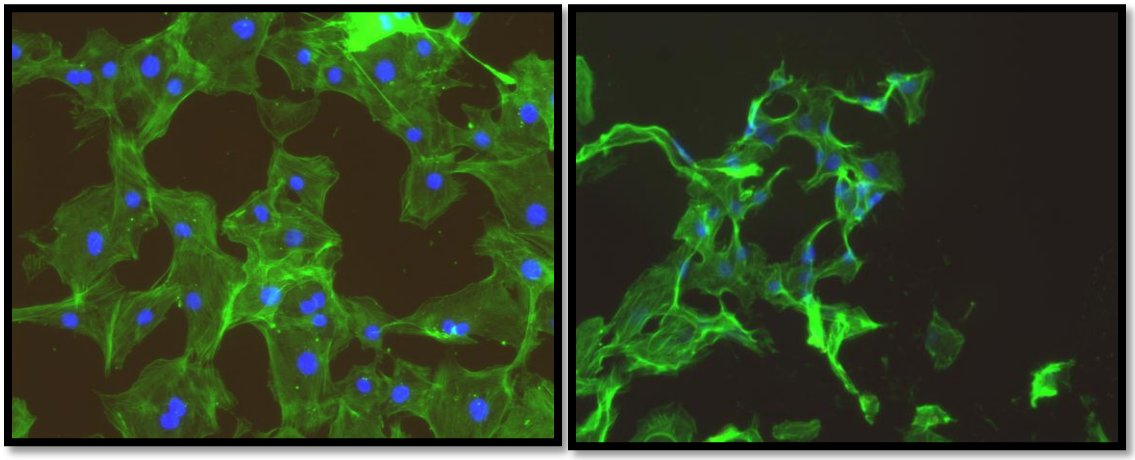

Figure 3.18. 0.2% pluronic F-68 Au NPs (left) and control solution (right)

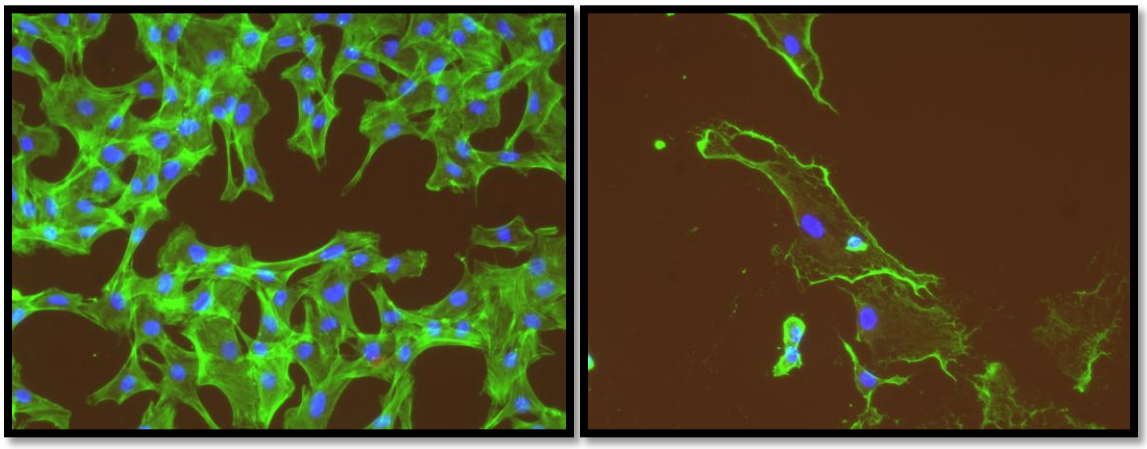

Figure 3.19. 1% pluronic F-68 Au NPs (left) and control solution (right)

The fluorescence images seen above show some important transitions between cells being treated with just the control solution and the NP capped solutions. The pluronic F68 treated cells show that the NP treated cells are much thicker than those treated with the control solutions. We also used different concentrations of pluronic F68 solutions to determine the effects of a change in concentration. The preliminary studies indicate that there may be a change caused by the concentration differences as the effects of the NP

and control solutions seem to be more pronounced with a higher concentration of pluronic F-68.

Discussion

The cells themselves aren't dying due to the NP treatment, which is a good start; however, the NPs are having an effect on the cells as a whole. The significant change in the elastic modulus as well as the morphology of the cells indicates the NPs are affecting the cytoskeleton. The cells are clearly being affected by the NPs and this is causing a change in the overall cell shape and mechanics. As seen in the immunofluorescence pictures the actin is forming different shapes inside the NP treated cells compared to the control untreated cells.

By showing that VSMCs are significantly affected by these NP systems this could potentially become problematic as these are the main type of cells associated with atherosclerosis. The NPs are sent systemically through the body at a quick pace and easily diffuse through the vessel walls, which make it easier for the cells to seek out cancer cells, but it also means they could interact with other healthy cells while in the circulation. These results show that this is likely another obstacle that will need to be addressed in developing nanoparticles that will be placed in the human body especially since many cells will be subjected to the particles. Unless the NPs can be targeted with 100% efficiency to a specific cell type then they will interact with other cells and possibly cause ill effects on healthy cells.

The exact mechanism by which nanoparticles affect cell mechanical properties and structure is not known and studies are underway to elucidate how nanoparticles can affect cell function.

Conclusions

The presence of NPs with VSMCs has clearly caused a shift in the mechanics as well as the morphology of the cells, yet they are not cytotoxic. Cells show a significant decrease in elastic modulus when treated with citrate capped NP systems as well as CMC NP systems. This is likely due to a disruption of actin synthesis in the cells making them have a lower modulus as actin filaments account for tension inside of the cell.

Further studies are being conducted to look at the actual protein regulation inside the cells before and after treatment with NPs to determine which phase, contractile or synthetic, the cells are in. Future studies will also be done looking at altering the size of the NP core and varying the core metal.

Acknowledgements

We would like to thank Brad Winn and Chaitra Cheluvaraju for their help with VSMC isolation techniques as well as Scott Wood for help with immunofluroescnce imaging and funding from NIH P20 RR-016461-09S1, NIH K25 HL092228, and HMMI SC LIFE.

CHAPTER 4

VARIOUS NANOPARTICLE EFFECTS ON DIFFERENT CELL TYPES

We also did several experiments with nanoparticles other than those reported in the previous chapter, specifically looking at cytotoxicity. These particles included green NPs that were capped by garlic and rosemary, magnetic NPs capped with dopamine and polyethylene glycol, and dodecanethiol.

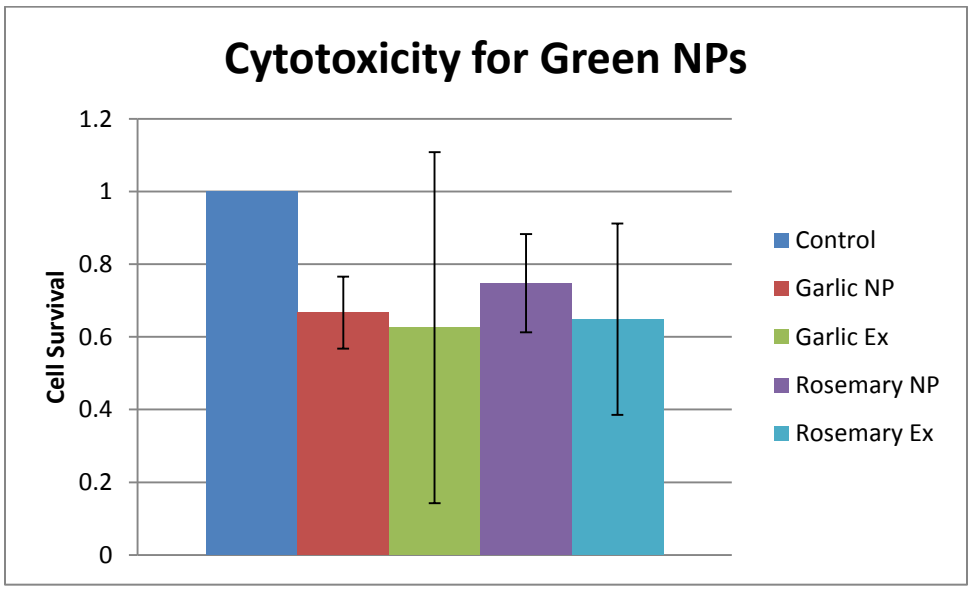

Table 4.1. Graph showing the amount of cell survival after treatment with garlic and rosemary capped NPs

Table 1 shows the cytotoxicity assay used to determine cell survival after treatment with garlic and rosemary capped NPs as well as extracts from each without NPs present. All the graphs in this chapter have the results normalized to the control which is 1. If the graphs show less than 1 that means some cells have died and if the graphs show a reading higher than one that means the cells were more proliferative than the control. The cells

used for this experiment were vascular smooth muscle cells. The results showed that a significant amount of cells died in all experimental groups except the garlic extract treated cells. This is believed to be caused because the concentration of the NPs was relatively high compared to other studies. This experiment was performed again on just garlic capped NPs with results seen below.

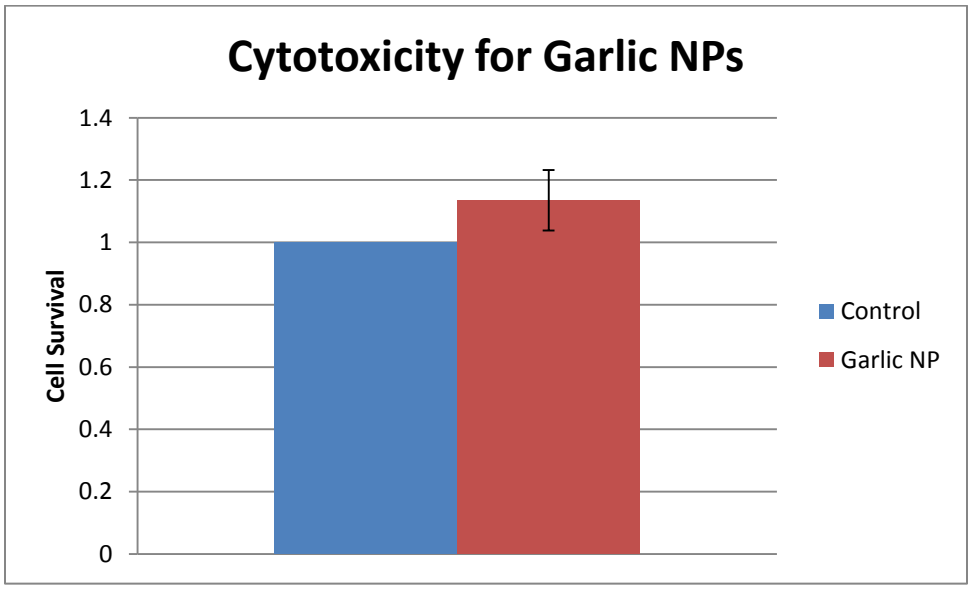

Table 4.2. Results of the second experiment performed on the garlic capped NPs

The results in table 2 are using a lower concentration of NPs before given to the cells and these initial results show that the cells actually proliferated more than the control untreated cells. The result could mean that the cells are shifting from a contractile state to a more synthetic state. The synthetic cells are more proliferative and would explain this result. Further imaging will be done to determine the phenotype of the treated cells.

We also looked at some magnetite NPs with the end goal of being able to treat cancerous cells with these particles and subject them to a magnetic field that would cause

them to heat up and trigger apoptosis in the diseased region. The original cytotoxicity test, which is what we did, will help us to know that the NPs can make it through the body targeted to a specific region without causing harm to other cells.

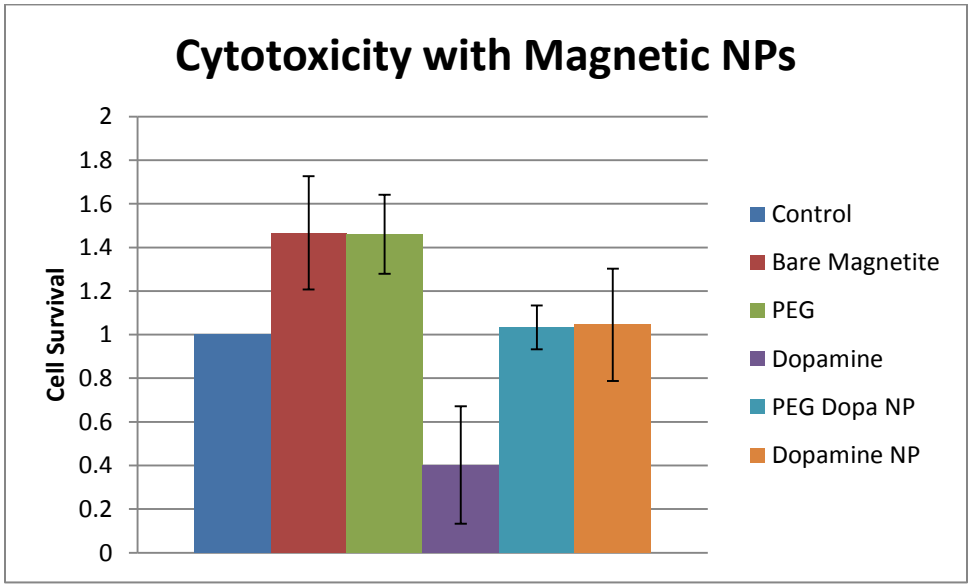

Table 4.3. Results of the cytotoxicity assay where cells were treated with magnetite capped NPs

The graph shown in Table 3 shows the only toxic treatment to be cells given dopamine, which is known to be cytotoxic in high concentrations. The cells used in this experiment were NIH 3T3 fibroblasts, and they are difficult to kill meaning that the dopamine was quite toxic to the cells. The capped NP treatments showed no significant change from the control, which is a plus for the overall goal of this project.

Similar experiments to the ones performed for the previous chapter were done with mesenchymal stem cells. In this assay we used citrate capped gold particles and

platinum capped CMC particles to assess cytotoxicity on stem cells that the NPs would encounter in the bloodstream.

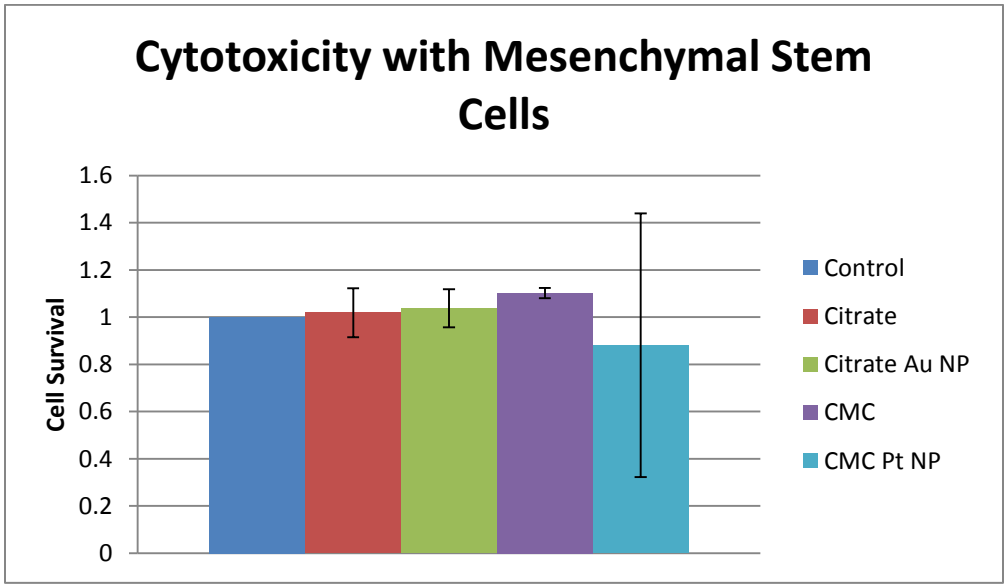

Table 4.4. Results of cytotoxicity assay on mesenchymal stem cells treated with gold and platinum NPs

The results seen in Table 4 indicate that none of the NPs were cytotoxic and the CMC extract actually showed a significant increase in cell number. These results prove helpful in that when NPs are injected into the human body they won't have ill effects on the circulating stem cells if they come in contact. When NPs are injected into an organism they will easily diffuse in and out of blood vessels and come in contact with many different cell types along their path.

Dodecanethiol particles were used because they are hydrophobic whereas all the other particles used are hydrophilic.

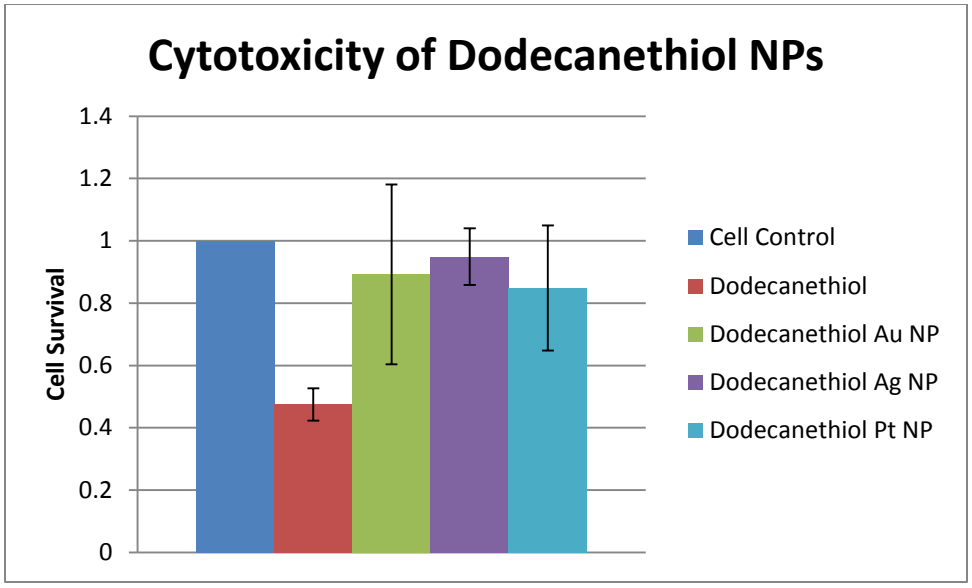

Table 4.5. Results of cytotoxicity assay showing cell survival after treatment with hydrophobic NPs

The different metals capped with dodecanethiol didn't have any effect on the cell survival, however the dodecanethiol itself killed a significant amount of cells.

All of these cytotoxicity results showed useful results in that they were positive towards the overall goal for each project. Green NPs are important because they don't require the use of an organic solvent during synthesis meaning that there is no possibility of that organic solvent being leftover due to inadequate wash steps. The magnetic NPs are not toxic to cells that they could pass while homing to a tumor, which would be a negative side effect. An important factor to note about the magnetic field application is that it can be applied locally, so even if some NPs interact with some cells elsewhere in the body they won't heat up when the magnetic field is applied making the system even safer to healthy cells. It is also important to look at stem cells as they are a natural repair

cell if things go wrong in the body, and our experiments show that if they do come in contact with the NPs we used they won't cause cell death, but further studies would need to be done to look any other possible damage.

CHAPTER 5

RECOMMENDATIONS

We have found some useful results from our experiments and there are still several directions to take the next step with this project. These steps include visualizing what the cells are doing with the NPs, Western Blotting to look for specific upregulated proteins, trying the same experiments with different metal cores of the NPs, and altering the size of the NPs.

In order to visualize the NPs in the cells we plan to utilize cryo-transmission electron microscopy. One of the benefits of this technique is the ability to look at our samples without having to fix or stain them which will allow us to view the cells in a natural state. We will be able to visualize what the cells are actually doing with the NPs. The cells may be congregating inside the cell while some may be attaching to the surface, and we will be able to determine exactly where the NPs are going.

The initial experiments done on this project have shown a significant change in the elastic modulus of VSMCs after treatment with gold nanoparticles through AFM testing. This needs to be further verified with Western Blots to determine if there is an upregulation in the contractile or synthetic markers inside the cells. These Western Blots will look for the expression of the proteins alpha-smooth muscle actin and smooth muscle-myosin heavy chain which are present in contractile VSMCs, and also to look for the upregulation of collagen type 1 and osteopontin which are proteins present in synthetic VSMCs. In order to effectively prove which phenotype the cells are there must be upregulation of two different proteins, and these four mentioned are the most prevalent

in each phenotype. The cytotoxicity testing shows that the NP treated cells aren't proliferating any different from the control cells and therefore we wouldn't expect the cells to have shifted towards the synthetic phenotype which is the proliferative cell type.

One other direction to take this research is to change the size and the metal of the core of the NPs. There have been some studies that look at the effects of the different sizes of NPs and how they react with organisms. Specifically, Chen et al. (Assessment of the In Vivo toxicity of gold NPs) showed that when they delivered different sizes of gold NPs to mice they obtained different results. The size range of 8 to 37 nm for their NPs in their study showed a significant increase in sickness in the mice while the particles that below 8 nm and above 37 nm showed no ill effects on the mice. Since the NPs used in our study were approximately 5 nm in diameter and showed no cytotoxicity, then we should try to increase the size of the particles to see if we can obtain similar results or if we start causing cells to die as well. The use of different metals would also help to give more insight looking at the effects beyond just gold, since gold is commonly used in many biomedical applications due to its biocompatibility. Silver would be interesting to look at due to its use as in antimicrobial applications like wound dressings.

Once these studies have been completed and depending on the results the project could move in to animal studies to look at specific tissues in the animals after being given NPs. Animal models are imperative to developing a technique that will be taken further towards clinical application. The NPs could be modified to home to a specific organ or tissue in the animal and then those tissues can be removed for further investigation

beyond just how the animals respond on the outside. The aorta could be removed to inspect the VSMCs since they are sure to come into contact with the NPs as they would be circulating in the blood and can pass through the blood vessels into other tissues.

A possible translatable goal for all of this research could be to ultimately develop a NP system that could target a scaffold in vivo and help in stem cell differentiation towards a specific fate needed. Seeing as so far our NP system appears to be safe in vitro and once more studies have been done looking into the Western Blots and altering the size and metal of the NP core, this system could serve as a novel exploration into the nanotechnology field in biomedical engineering.

Appendices

Appendix A

Isolating Vascular Smooth Muscle Cells

- Sacrifice rat using CO2 asphyxiation and cervical dislocation
- Remove aorta from subclavian origin to the diaphragm bifurcation and place in DMEM with pen/strep
- Use tissue culture hood to remove all adventitia and connective tissue. All adventitia must be removed to ensure you only attain VSMCs
- Cut vessel longitudinally so it lays flat and scrape off endothelium gently with scalpel blade and rinse thoroughly in DMEM with pen/strep
- Cut the vessel into ~5 mm squares and place them in digestion solution that includes 5 ml DMEM, pen/strep (1%), Collagenase type II (final concentration 175U/ml), and 10% FBS for 20 minutes
- Centrifuge at 500 rpm for 1 minute and remove the supernatant and wash the pellet with DMEM containing pen/strep
- Resuspend the pieces in another digestion solution containing DMEM, pen/strep (1%) Collagenase type II (final concentration 175U/ml), Elastase type III (final concentration 0.25 mg/ml) and 10% FBS for 1 hour. Be sure to shake the tube gently every 10 minutes until the vessel is gossamer thin. When the vessels are dissolved stop the digestion by diluting with equal volume of DMEM with pen/strep and 20% FBS
- Centrifuge 1000 rpm for 5 minutes and remove the supernatant

- Suspend cells in DMEM with pen/strep and 20% FBS and place in T-25 flask and put in incubator (37C, 5% CO2). Don't change media for 72 hours as cells need sufficient time to adhere to flask.
- Maintain the cells using DMEM with 20% FBS and pen/strep until cells reach P4 then use 10% FBS

Appendix B

Modeling and Experimental Measurement of Thermal Diffusion Across Human Teeth Due to Drilling and other Restorative Procedures

Abstract:

Many dental restorative procedures require the removal of enamel and/or dentin. Although there are several methods to remove damaged material, drills remain the most common. The dental bur, a type of drill bit, sliding contact with the hard tissues can cause it to act as a heat source within the tooth. This paper builds on previous studies to build two models of heat transfer through a tooth using COMSOL, a finite element solver. One model is based on the heat transversing an intact tooth and the other is of a sliced tooth. The purpose of the sliced tooth is to limit the processing power needed to run the model. Both the computation models and experiments measured how a point source of heat (ranging from 50-70 °C) altered the temperature of surrounding hard tissue temperature. Comparisons between experimental data and the models show that the tooth slices were found to heat up more slowly than predicted by the FEM model. However, the intact tooth model showed good agreement with the experimentally measured heating curve of the intact teeth. In addition, these models showed moderate agreement with an analytical 1D heat transfer model.

Introduction:

The human tooth is a complex structure of interlaced hard tissues, enamel and dentin. Many studies have been devoted to restoring these tissues when decay or damage

begins to occur. This has resulted in the development of novel materials for fillers to help restore the mechanical integrity of the tooth. Additional work, however, is still needed to improve this process and also the understanding of the enamel/dentin properties and junction. The cross-section in Figure 1, clearly shows the delineation between these two tissues. Enamel is a very hard material composed primarily of hydroxylapatite and offers excellent wear resistance. The dentin, found just below the enamel, is tough and highly elastic material, that is also composed of hydroxylapatite mixed with a larger percentage of proteins (mainly collagen type 1).

Many restorative dental operations, from the removal of dental caries to the excision of broken teeth, require the use of a dental drill (with a specialized bit typically referred to as a "bur").(1-3) Today, these drills are sometimes referred to as high-speed hand-pieces (HSPS). Doctors and dentists have long been aware that drills-generated heat can cause damage to mineralized tissues (e.g., bones and teeth). The earliest recording of temperature sensitivity of teeth to drilling heat was made in 500 B.C.E., when Hippocrates advocated drilling slowly and extracting the drill frequently to submerge it in water to decrease the temperature.(4) When a dental bur is used to remove tooth material, the friction between the bur and the tooth can generates a significant amount of heat. The speed, selection of bur, etc can control the amount of heat generated when using a HSHP. Although, there are no citations as to the temperatures reached during the drilling of teeth, drill burs have been estimated to reach temperatures ranging from 49°C to 115°C while boring within bone.(5, 6) From the normal body temperature of 37°C, a temperature increase to only 48°C could possibly damage a tooth beyond

repair.(7) Previous studies have shown that bone cells are severely damaged at temperatures as low as 40°C, and they undergo necrosis at temperatures around 50°C.(4, 8) Dental pulp, the part of the tooth that contains the blood vessels necessary to keep the tooth alive, usually undergoes necrosis with a temperature increase of only 11.1C°.(9, 10)

Previous studies related to heat transfer in teeth have largely focused on quantifying the thermal properties of teeth – such as specific heat (energy required to heat a certain mass of material by 1°C), thermal conductivity (measure of a material's ability to transport heat), thermal diffusivity, and density (mass per unit volume).(4) In 1961, Craig and Peyton (5) first looked into the thermal conductivity of enamel, dentin, dental cements and amalgam. Later in 1970, the Brown, Dewey, and Jacobs (11) built upon Craig and Peyton's findings to quantify the specific heat of dentin and enamel, also shown in Table 1. Focus of research groups, such as Magalhães et al (9), switched to eliminating the error and range of results of the thermal conductivity. Their worked showed that the newer "flash laser method" yielded a narrower range of thermal conductivity constants for dentin.

For this reason, an average of their values for the thermal conductivity and specific heat of dentin was used in this study. As a comparison, the data was also compared to the analytical one-dimensional heat transfer equation (9, 12):

$$\theta(t) = (1 - e^{-\frac{h}{\rho C_p L}t})\frac{q}{h} \quad (1)$$

where θ is the magnitude of temperature rise above room temperature (25°C); t is the time; ρ is the density; C_p is the specific heat; L is the distance that the heat must travel (the width of the tooth); h is the heat transfer coefficient, and q is the heat supply. The heat transfer coefficient can be found by dividing the thermal conductivity, k, by the distance across which the heat is conducting. The heat supply is calculated normalizing the thermal conductivity by the distance.

Although much work has focused on measurement of the thermal properties of dental tissue, there is a critical need for improved mathematical modeling of the temperature distribution within teeth.(11, 13) Accurate computer modeling of heat propagation in teeth will lead to a better understanding of bur-generated heat damage in teeth. Finite element analysis has been used recently to examine thermal effects of drilling in bone but not yet on teeth.(8, 14) This study aims to model the thermal properties of teeth in various environments by using Finite Element Modeling (FEM) simulations to better assess the possible damage done to dental cells by drill bur-generated heat. Simulations were performed using COMSOL Multiphysics (Heat Transfer Module) of both intact slices and also 2 mm thick tooth slices.

Methods and Materials:

Computational Modeling of Heat Transfer

Finite element models (FEM) of the heat transfer across both an intact tooth and also a tooth slice were made using COMSOL, a finite element solver. The purpose of each model was to simulate the spatial temperature distribution within the hard tissues in order to better understand the heat transfer. The size and geometry were made to match

scans taken by micro-computed tomography of each tooth and the *Intact Tooth* model (model taking into account a whole tooth) file had a mesh with approximately 28,000 elements. The parameters used to generate heating curves included the tooth densities, thermal property parameters averaged from literature reports. Plots of temperature and time at the point selected in the tooth at a given distance from the hotplate were constructed. For all of the plots, the point selected corresponded to the location of the thermal probe. All the same assumptions were made for the tooth slice FEM model, which had a mesh of approximately 1,000 elements. Both of these models will also be compared to the analytical solution depicted by equation 1. The parameters used for this equation are shown in Table 2.

Tooth Selection

The human teeth used in this experiment were extracted at the Medical University of South Carolina Dental School and contained either localized caries or vertical cracks. Specimens with abnormal features, such as cracks, cavities, fillings, etc. in the vicinity of the testing area were eliminated. A total of 14 teeth were used in this study, eight for comparison with the Intact Tooth FEM Model and six teeth with the Slice FEM model. All the teeth were treated with 5% Chloramine solution for 12 hrs and then transferred to Clemson University where they were stored in Hank's Balanced Salt Solution (HBSS). (15, 16) Density was experimentally determined for each tooth by using a mass balance and a volume measurement. All intact teeth and slices were removed from the HBSS and briefly air-dried for 30 seconds prior to testing.

Preparation of Teeth Samples

To measure heat conduction to the center of intact teeth, six individual intact tooth samples were drilled by a Craftsman drill press along the root canal in the center of the tooth. Some teeth were also sectioned. To facilitate handling during sectioning, three teeth were embedded in non-infiltrating Caroplast embedding media. 2mm thick sections were cut an Isomet 4000 Linear Precision Saw. The drilled and sectioned samples were then placed on a VWR VMS-C7 hot plate having a temperature of 50-70 °C. Both the temperature of the hotplate and tooth was measured using two K-type thermocouples and a wireless high-accuracy thermocouple thermometer (Omega HH802W). The thermocouple measuring dental heating was either inserted inside the drilled canal of the intact tooth samples or positioned on top of the sectioned samples. The heating curve for each sample was recorded using the wireless computer recording software of the HH802W. This experimental setup is shown in Figure 2. When the tooth slices were not in use, they were stored in a dry Petri dish in a refrigerator, while the drilled teeth were stored in HBSS.

Results and Discussion:

For both the full tooth model and the tooth slice model, the values used for the enamel were taken from the work of Brown (17) and the values for the dentin were taken from an average of the values found by Magalhães (9). The density was measured to be 2700g/m^3 and was found to be within the range found in previous studies. (9, 17) In the present study, the dental pulp tissue was not analyzed, as all teeth used in this study were cleaned and disinfected with chloramines to avoid transportation of biohazards.

Measurement of Heat Transfer Across Intact Teeth

Although there was variation among the eight intact teeth tested, the teeth tended to follow similar heating patterns and the standard deviation was relatively small. The center of teeth tested reached 40°C within 50 to 100 seconds. This indicates that dangerous levels of heat could easily reach the pulp within times relevant for dental procedures.

Modeling of Heat Transfer Across Intact Teeth

A 3D finite element model using COMSOL using the average values listed in Table 1. Figure 3 shows the Intact Tooth model. The color over the mesh shows the heat distribution through the modeled tooth. This model was validated by comparing to a temperature curve that showed temperature as a function of time at a given point, such as in Figure 4.

Finally, to test the full tooth model's accuracy, it was used to simulate a tooth being heated to 70°C for 200 sec and then cooled at 25°C for 400 seconds. The final test, in which the model was used to predict the cooling time of the tooth, displayed that the model cooled down more slowly than the real teeth. While this shows that the model is slightly inaccurate, the slower cooling time could be advantageous. If a dentist were to use this model to track the heating and cooling of a tooth during drilling, it would protect the human tooth by cooling down slower than the real tooth would. This error, although minor, could be attributed to the presence of pulp in the real teeth, which was absent in the model, as well as the porosity of the dentin. Manipulating the specific heat in the

FEM model could remedy this problem. Until further work is done, the literature-based model can be used to model the first 200 seconds of a full tooth heating at 70 °C.

Measurement and Modeling of Heat Transfer Across Sliced Tooth Sections

Heat transfer across a tooth was modeled using both analytical and finite element models. The mesh of the Slice FEM model and temperature gradient produced when a room temperature slice is put in contact with a 50 °C is shown in Figure 5.Figure 6 shows the prediction of the Slice model along with the temperature curves of six tooth slices. The double layer of dentin and enamel in the tooth can possibly offer an explanation for this difference between the real teeth and the model – the heat may travel through the enamel and then slow down when it reaches the less thermally conductive dentin.

The analytical model followed the heating of the tooth well enough to be used as a general model, but it should be noted that the analytical model differs from both the actual data and the finite element model for the first ten to twenty seconds. While slopes of the curves for the FEM model and the actual teeth do not begin to seriously increase until ten twenty seconds have passed, the analytical model immediately begins to increase. This discrepancy between the analytical and FEM models is due to the more complex 3D geometry of the tooth which is captured by the FEM model but not reflected with the 1D analytical solution. However, the analytical model is a very simple calculation, which makes it easier to compute than the using full finite element computation.

Comparison of Slice and Intact FEM Models

As stated in the methods section, the analytical model followed the curve of the following one-dimensional heat transfer equation. The large error with the literature value-based model in the tooth slice experiment could possibly be attributed to the anisotropic characteristics of teeth, as well as the fact that the tooth slices were stored in a dry environment. The heating experiment was also performed on some tooth slices while they were within the caroplastic, which may also have affected the rate at which the slice heated up. However, even though the literature model did not match the heating curve of the tooth slice, the literature model matched the heating curve of the real teeth in the full tooth experiment reasonably well. The full tooth experiment more accurately replicates the drilling of a human tooth *in vivo*, so the literature-based model may still be used. The graph below is taken from the three-curve graph above, but it focuses on the first 60 seconds of heating to show the difference in heating times between the two models. It should be noted that the material properties in the finite element model were still isotropic and, therefore, did not account from the dentin anisotropy.

Extraction of Thermal Conductivity and Specific Heat Parameters

The parameters averaged from literature numbers caused the model to heat up too slowly for the tooth slices, but accurately followed the heating curve of the full tooth for the first 200 seconds; this irregularity within the tooth slice experiment could possibly be attributed to the anisotropic characteristics of teeth, the double layer of dentin and enamel in the tooth, and the porosity of the dentin. The thermal conductivity and specific heat then were varied for both the enamel and the dentin to fit the model-generated curve to

the experimental data curve. After initial comparison of model to the experimental data, the thermal conductivity and specific heat were allowed to float to allow force the model to obtain a closer fit to the heat transfer experimental data. The initial and fit parameters values are summarized in Table 3.

Conclusions:

There are many factors that prohibit the development of a conclusive computational model. These include the following: (1) the thermal properties of each tooth vary by type (incisor, canine, molar) and also the donor identifying factors (age, health, sex, etc), (2) the boundary conditions such as the soft tissues, bone, etc are too complex to model.

Acknowledgements:

The authors would like to thank L. Datko, B. Zimmerman, C. Peay, S. Deitch, S. Wood and M. Cupelli for their helpful discussions. They would also like to thank L. Jenkins for sample preparation and M. Lemus for micro-computed tomography discussions. This project was funded grants from the Howard Hughes Institute for both the Clemson Summer Program for Research Interns and SC Life program.

Figure and Tables with Captions:

(A) 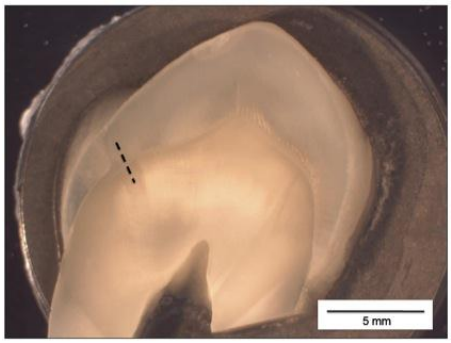

(B) 

Figure 1: a) This optical image is of a representative tooth cross-section used for slice experiments. This image clearly shows the outer enamel layer and inner dentin layer. b) a cross-section of a micro-CT image of one of the intact teeth used in this study showing the drilled area in which the thermocouple probe was inserted.

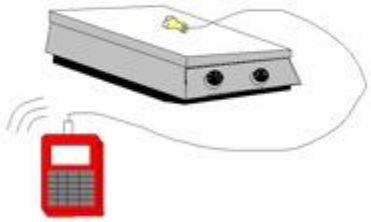

Figure 2: This schematic shows the experimental heat transfer set up. Either a drilled or sliced tooth (at room temperature) was placed on hotplate (having a shelf temperature of approximately 50-70°C). Both the temperature of the hotplate and tooth were measured with thermocouples.

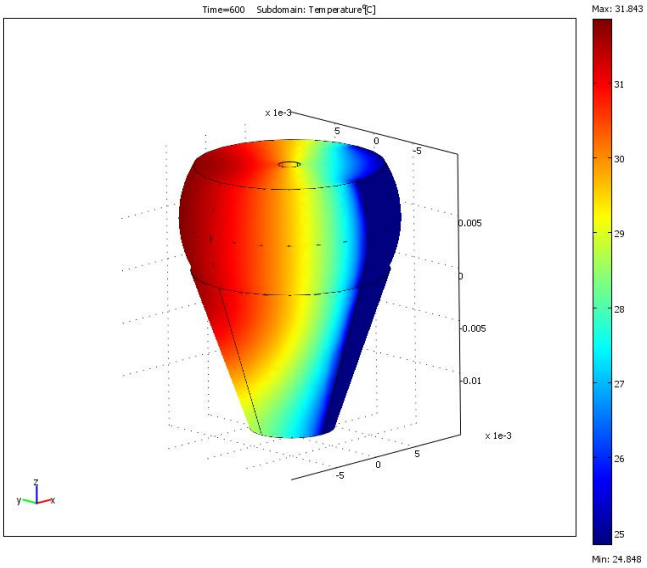

Figure 3: Spatial temperature distribution using the *Intact Tooth* FEM model. This simulation show the temperature gradient when a tooth (initially at 23°C) is put in contact with a 70°C surface and held for 600 sec.

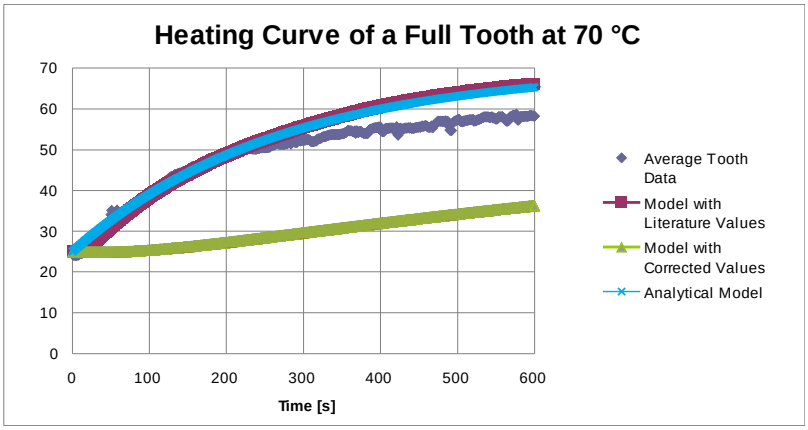

Figure 4: By comparing the temperature predicted by the Intact Tooth FEM model to the temperature experimentally by the thermocouple on the inside of the tooth, the model is shown to accurately predict the temperature up during the first 200 sec of exposure to the 50°C point source. The experimental data is the average of data from six full teeth

samples. Surprisingly, the analytical 1D model shows close agreement with the Intact Tooth FEM model after 100 sec.

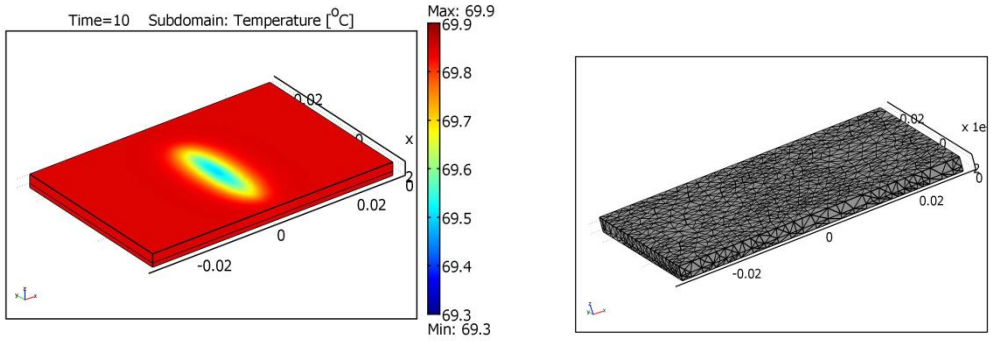

(A) (B)

Figure 5: (A) This is the simulation of the *Sliced Tooth* FEM model. The simulation shows of the tooth slice encased in a block of air, heated to 50°C. (B) The model mesh.

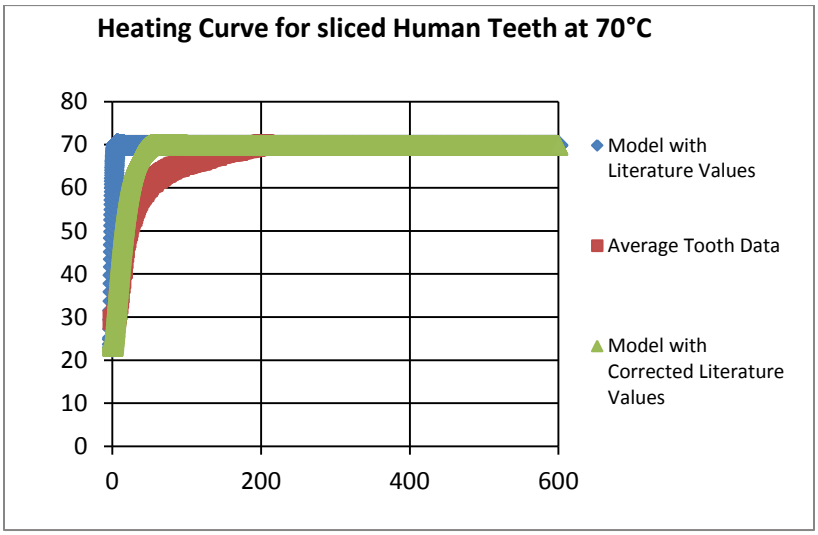

Figure 6: By comparing the temperature predicted by the Slice FEM model to the temperature experimentally by the thermocouple on top of the tooth slice and heat source is 50°C, the model is shown to accurately predict the temperature up during the first 100

sec of exposure to the 50°C point source. Again, the analytical 1D model shows close agreement with the Slice FEM model.

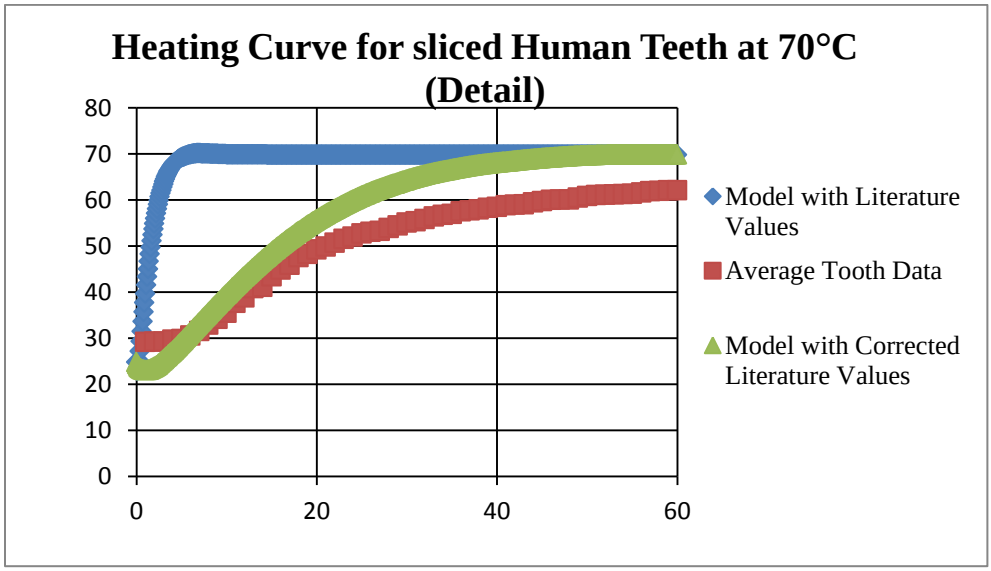

Figure 7: This graph shows both the temperature predicted by the Slice FEM model and the temperature experimentally measured by the thermocouple on top of the tooth slice when the heat source is 70°C. The parameters used in the FEM model were from Table 3.

	Enamel Component			Dentin Component			Whole Tooth		
	Average Value	Reported Value	Reference	Average Value	Reported Value	Reference	Average Value	Reported Value	Reference
Thermal Conductivity -k- (W/(m-K))	0.9	0.93	Craig and Peyton	0.5572	0.58	Craig and Peyton	-		
		?	?		0.36	Magalhães			
					0.48-0.66	Magalhães			
Density -ρ- (kg/m^3)	2700	?	?	2000	2090-2400	Magalhães	2200	2200	Brown
		?	?		?	?			
Specific Heat -c_p- (J/(g-K))	700	710	Brown	1066	1590	Brown	1260	1260	Brown
		?	?		870	Magalhães			
					1040-1180	Magalhães			

Table 1: Previous groups have experimentally measured the thermal conductivity, density and specific heat of both Dentin and Enamel. This table contains the average values of three commonly cited studies. (5, 9, 17)

	Enamel		**Dentin**	
	Initial Model Parameters	Model Parameters after fitting to data	Initial Model parameters	Model Parameters after fitting to dat
Thermal Conductivity (W/(m-K))	0.9	0.3	0.5572	0.108
Density (kg/m^3)	2700	2700	2000	2000
Specific Heat (J/(g-K))	700	1500	1066	2000

Table 2: Parameters used in analytical 1-D model that was compared to both the slice and intact tooth FEM models. All parameters are for dentin and are the averages of values reported in literature. (5, 9, 17)

Heat Flux	Mass of Tooth Slice	Density of Tooth	Specific Heat	Distance from Heat Source	Heat Transfer Coefficient	Thermal Conductivity
q	m	ρ	C_p	L	h	k
(W/m^2)	kg	(kg/m^3)	(J/(g C))	(m)	$(W/(m^2\text{-}C))$	$(W/(m^2\text{-}sec))$
45	0.004	2000	1066	0.0085	67.88235	0.577

Table 3: By fitting the intact tooth FEM model to the experimentally measured temperature profiles, the model parameters (thermal conductivity, density and specific heat) solved for. This table shows the variation between these parameter values and those reported in other studies.

References:

1. Siegel SC, Von Fraunhofer JA. Effect of handpiece load on the cutting efficiency of dental burs *Machining Science and Technology: An International Journal* 1997;**1**(1):1 - 13.

2. Siegel SC, VonFraunhofer JA. Dental cutting: The historical development of diamond burs *J Am Dent Assoc* 1998;**129**(6):740-745.

3. Banerjee A, Watson TF, Kidd EAM. Conservative dentistry: Dentine caries excavation: a review of current clinical techniques. *Br Dent J* 2000;**188**(9):476-482.

4. Karmani S. The thermal properties of bone and the effects of surgical intervention. *Current Orthopaedics* 2006;**20**(1):52-58.

5. Craig RG, Peyton FA. Thermal Conductivity of Tooth Structure, Dental Cements, and Amalgam. *Journal of Dental Research* 1961;**40**(3):411-418.

6. Chacon GE, Bower DL, Larsen PE, McGlumphy EA, Beck FM. Heat Production by 3 Implant Drill Systems After Repeated Drilling and Sterilization. *Journal of Oral and Maxillofacial Surgery* 2006;**64**(2):265-269.

7. Baldissara P, Catapano S, Scotti R. Clinical and histological evaluation of thermal injury thresholds in human teeth: a preliminary study. *Journal of Oral Rehabilitation* 1997;**24**(11):791-801.

8. Giraud JY, et al. Bone cutting. *Clinical Physics and Physiological Measurement* 1991;**12**(1):1.

9. Magalhaes MFd, Ferreira RAN, Grossi PA, Andrade RMrd. Measurement of thermophysical properties of human dentin: Effect of open porosity. *Journal of Dentistry* 2008;**36**(8):588-594.

10. Zach L, Cohen G. Pulp response to externally applied heat. *Oral Surgery, Oral Medicine, Oral Pathology* 1965;**19**(4):515-530.

11. Jacobs HR, Thompson RE, Brown WS. Heat Transfer in Teeth. *Journal of Dental Research* 1973;**52**(2):248-252.

12. Ozisik MN. Heat Transfer: A Basic Approach, 1st Edition. Burr Ridge, IL: McGraw-Hill Companies, 1984.

13. Panas AJ, Żmuda S, Terpiłowski J, Preiskorn M. Investigation of the Thermal Diffusivity of Human Tooth Hard Tissue. *International Journal of Thermophysics* 2003;**24**(3):837-848.

14. Davidson SRH, James DF. Drilling in Bone: Modeling Heat Generation and Temperature Distribution. *Journal of Biomechanical Engineering* 2003;**125**(3):305-314.

15. Habelitz S, Marshall Jr GW, Balooch M, Marshall SJ. Nanoindentation and storage of teeth. *Journal of Biomechanics* 2002;**35**(7):995-998.

16. Zimmerman B, Datko L, Cupelli M, Alapati S, Dean D, Kennedy M. Alteration of dentin-enamel mechanical properties due to dental whitening treatments. *Journal of the Mechanical Behavior of Biomedical Materials* 2010;**3**(4):339-346.

17. Brown WS, Dewey WA, Jacobs HR. Thermal Properties of Teeth. *Journal of Dental Research* 1970;**49**(4):752-755.

Appendix C

MATLAB Scripts

Hertz Model Analysis for Batch Export from MFP3-D AFM machine (reads text files generated by the computer)

```
function elasticity = massexcompile(folderin)
mainfolder = cd
format long
fnames = dir(folderin);
numfids = length(fnames);
cd(folderin);
%filtering out irrelevent "files" such as '.' and '..'
cellnames = {};
for c = 1:numfids;
    if 'C' == fnames(c).name(1) % 'C' represents the letter that the
relevent file names begin with
        cellnames{end+1} = fnames(c).name;
    end
end
%combine every 3 files and write
counter = 1;
numcell = length(cellnames);
numfile = 1;
elasticity = [];

% OMIT THIS WHILE LOOP IF YOU WANT TO LOAD CELLS INDIVIDUALLY
while counter <= numcell
    a = load(cellnames{counter});
    c = load(cellnames{counter+2});

    cd(mainfolder);
    elasticity(end+1,[1,2]) = elast_analysis(c,a,mainfolder);
    counter = counter+3;
    cd(folderin);
    %numfile = numfile+1
end


function e = elast_analysis(c,a,mainfolder)
cd(mainfolder)
format long
k = 0.1416; %spring constant value N/m
v = 0.5; %poisson's ratio
R = 2.5*10^-6;  % tip radius in meters
L = 10*10^-9 ;     %lower bound for elasticity (in m from contact
point)
```

```
U = 700*10^-9 ;   %upper bound for elasticity (in m from contact point)


%adjust deflection
ak = a.*k;
%filter deflection values
d = AFM_butter(ak);
%Separation of extension and retraction
l = floor(length(c)/2);
xe = c(200:l);% add 200 in order to omit first several data points
(irratic behavior due to filtering
ye = d(200:l);
if rem(length(c),2)==0;
    xr = c(end-200:-1:l+1); % subtract 200 in order to omit first
several data points
    yr = d(end-200:-1:l+1);
    else
    xr = c(end-200:-1:l+2);
    yr = d(end-200:-1:l+2);
end

%correct x,y offsets
[xe,ye] = xycorrect(xe,ye);
[xr,yr] = xycorrect(xr,yr);



format long;
erange = [];
for i = [1:1:length(xe)];
    if xe(i)>=L && xe(i)<=U;
        erange(end+1) = i;
    end;
end;
rrange = [];
for i = [1:1:length(xr)];
    if xr(i)>=L && xr(i)<=U;
        rrange(end+1) = i;
    end;
end;


emodulus = mean((3.*ye(erange).*(1-
v^2))./(4.*xe(erange).^(3/2).*R.^(1/2)));
rmodulus = mean((3.*yr(rrange).*(1-
v^2))./(4.*xr(rrange).^(3/2).*R.^(1/2)));

e = [emodulus, rmodulus];


function [i] = AFM_butter(x) %applies butterworth filter to data
format long
```

```
[b,a]=butter(3,.025);
i=filter(b,a,x);


function [xc,yc] = xycorrect(x,y)
s = 0.002; %slope sensitivity


%correction for y
format long
region = [1:length(x)/4];
slope = polyfit(x(region),y(region),1);
yci = y-(slope(1).*y);

%correction for x
numslope = diff(yci)./diff(x);
index = 1;
condition = 0;
contactx = 0;
while condition == 0 && index ~= length(numslope)
    if numslope(index) > s && mean(numslope(index:5:index+200)) > s;
        condition = 1;
        contactx = index;
    end
    index = index+1;
end
xc = x-x(contactx);

% correct again for y
yc = yci-yci(contactx);
```

REFERENCES

1. Gwinn MR, Vallyathan V. Nanoparticles: Health Effects-Pros and Cons. *Environmental Health Perspectives*. 2006;(12):1818-1825. Available at: http://ehp.niehs.nih.gov/docs/2006/8871/abstract.html.

2. Kagan VE, Bayir H, Shvedova A a. Nanomedicine and nanotoxicology: two sides of the same coin. *Nanomedicine : nanotechnology, biology, and medicine*. 2005;1(4):313-6. Available at: http://www.ncbi.nlm.nih.gov/pubmed/17292104.

3. Emerich DF, Thanos CG. The pinpoint promise of nanoparticle-based drug delivery and molecular diagnosis. *Biomolecular engineering*. 2006;23(4):171-84. Available at: http://www.ncbi.nlm.nih.gov/pubmed/16843058.

4. Pernodet N, Fang X, Sun Y, et al. Adverse effects of citrate/gold nanoparticles on human dermal fibroblasts. *Small (Weinheim an der Bergstrasse, Germany)*. 2006;2(6):766-73. Available at: http://www.ncbi.nlm.nih.gov/pubmed/17193121.

5. Goodman CM, McCusker CD, Yilmaz T, Rotello VM. Toxicity of gold nanoparticles functionalized with cationic and anionic side chains. *Bioconjugate chemistry*. 2004;15(4):897-900. Available at: http://www.ncbi.nlm.nih.gov/pubmed/15264879.

6. Connor EE, Mwamuka J, Gole A, Murphy CJ, Wyatt MD. Gold nanoparticles are taken up by human cells but do not cause acute cytotoxicity. *Small (Weinheim an der Bergstrasse, Germany)*. 2005;1(3):325-7. Available at: http://www.ncbi.nlm.nih.gov/pubmed/17193451.

7. Shukla R, Bansal V, Chaudhary M, et al. Biocompatibility of gold nanoparticles and their endocytotic fate inside the cellular compartment: a microscopic overview. *Langmuir : the ACS journal of surfaces and colloids*. 2005;21(23):10644-54. Available at: http://www.ncbi.nlm.nih.gov/pubmed/16262332.

8. Chen Y-S, Hung Y-C, Liau I, Huang GS. Assessment of the In Vivo Toxicity of Gold Nanoparticles. *Nanoscale research letters*. 2009;4(8):858-864. Available at: http://www.pubmedcentral.nih.gov/articlerender.fcgi?artid=2894102&tool=pmcentrez&rendertype=abstract

9. Marchal F, Pic E, Pon T, et al. F. Quantum dots in oncological surgery: the future for surgical margin status? *Bulletin du Cancer* 2008;95: 1149–1153. Available at: http://www.ncbi.nlm.nih.gov/pubmed/19091647

10. Patra CR, Bhattacharya R, Mukhopadhyay D, Mukherjee P. Fabrication of gold nanoparticles for targeted therapy in pancreatic cancer. *Advanced drug delivery reviews*. 2010;62(3):346-61. Available at: http://www.pubmedcentral.nih.gov/articlerender.fcgi?artid=2827658&tool=pmcentrez&rendertype=abstract

11. Cuenca AG, Jiang H, Hochwald SN, et al. Emerging implications of nanotechnology on cancer diagnostics and therapeutics. *Cancer*. 2006;107(3):459-66. Available at: http://www.ncbi.nlm.nih.gov/pubmed/16795065

12. El-Sayed IH, Huang X, El-Sayed M a. Surface plasmon resonance scattering and absorption of anti-EGFR antibody conjugated gold nanoparticles in cancer diagnostics: applications in oral cancer. *Nano letters*. 2005;5(5):829-34. Available at: http://www.ncbi.nlm.nih.gov/pubmed/15884879.

13. El-Sayed IH, Huang X, El-Sayed M a. Selective laser photo-thermal therapy of epithelial carcinoma using anti-EGFR antibody conjugated gold nanoparticles. *Cancer letters*. 2006;239(1):129-35. Available at: http://www.ncbi.nlm.nih.gov/pubmed/16198049.

14. Hirsch LR, Stafford RJ, Bankson J a, et al. Nanoshell-mediated near-infrared thermal therapy of tumors under magnetic resonance guidance. *Proceedings of the National Academy of Sciences of the United States of America*. 2003;100(23):13549-54. Available at: http://www.pubmedcentral.nih.gov/articlerender.fcgi?artid=263851&tool=pmcentrez&rendertype=abstract

15. Loo C, Lowery A, Halas N, West J, Drezek R. Immunotargeted nanoshells for integrated cancer imaging and therapy. *Nano letters*. 2005;5(4):709-11. Available at: http://www.ncbi.nlm.nih.gov/pubmed/15826113.

16. Wang M, Thanou M. Targeting nanoparticles to cancer. *Pharmacological research : the official journal of the Italian Pharmacological Society*. 2010;62(2):90-99. Available at: http://www.ncbi.nlm.nih.gov/pubmed/20380880.

17. Schweiger C, Pietzonka C, Heverhagen J, Kissel T. Novel magnetic iron oxide nanoparticles coated with poly(ethylene imine)-g-poly(ethylene glycol) for potential biomedical application: Synthesis, stability, cytotoxicity and MR imaging. *International journal of pharmaceutics*. 2011:1-8. Available at: http://www.ncbi.nlm.nih.gov/pubmed/21315813.

18. Das RK, Gogoi N, Bora U. Green synthesis of gold nanoparticles using Nyctanthes arbortristis flower extract. *Bioprocess and biosystems engineering*. 2011. Available at: http://www.ncbi.nlm.nih.gov/pubmed/21229266.

19. Leonard K, Ahmmad B, Okamura H, Kurawaki J. In situ green synthesis of biocompatible ginseng capped gold nanoparticles with remarkable stability. *Colloids and surfaces. B, Biointerfaces*. 2011;82(2):391-6. Available at: http://www.ncbi.nlm.nih.gov/pubmed/20980131.

20. Kumar A, Chaudhry I, Reid MB, Boriek AM. Distinct signaling pathways are activated in response to mechanical stress applied axially and transversely to skeletal muscle fibers. *The Journal of biological chemistry*. 2002;277(48):46493-503. Available at: http://www.ncbi.nlm.nih.gov/pubmed/12221078.

21. Suzuma I, Suzuma K, Ueki K, et al. Stretch-induced retinal vascular endothelial growth factor expression is mediated by phosphatidylinositol 3-kinase and protein kinase C (PKC)-zeta but not by stretch-induced ERK1/2, Akt, Ras, or classical/novel PKC pathways. *The Journal of biological chemistry*. 2002;277(2):1047-57. Available at: http://www.ncbi.nlm.nih.gov/pubmed/11694503.

22. Keila S, Pitaru S, Grosskopf A, Weinreb M. Bone Marrow from Mechanically Unloaded Rat Bones Expresses Reduced Osteogenic Capacity In Vitro. *Journal of Bone and Mineral Research*. 1994;9(3):321-327.

23. Wang F-S, Wang C-J, Sheen-Chen S-M, et al. Superoxide mediates shock wave induction of ERK-dependent osteogenic transcription factor (CBFA1) and mesenchymal cell differentiation toward osteoprogenitors. *The Journal of biological chemistry*. 2002;277(13):10931-7. Available at: http://www.ncbi.nlm.nih.gov/pubmed/11784711.

24. Lin C-Y, Chang F-H, Chen C-Y, et al. Cell therapy for salivary gland regeneration. *Journal of dental research*. 2011;90(3):341-6. Available at: http://www.ncbi.nlm.nih.gov/pubmed/21297017

25. Wang Q, Jamal S, Detamore MS, Berkland C. PLGA-chitosan/PLGA-alginate nanoparticle blends as biodegradable colloidal gels for seeding human umbilical cord mesenchymal stem cells. *Journal of biomedical materials research. Part A*. 2011;96(3):520-7. Available at: http://www.ncbi.nlm.nih.gov/pubmed/21254383

26. Elsherbini A a M, Saber M, Aggag M, El-Shahawy A, Shokier H a a. Magnetic nanoparticle-induced hyperthermia treatment under magnetic resonance imaging. *Magnetic resonance imaging*. 2011;29(2):272-80. Available at: http://www.ncbi.nlm.nih.gov/pubmed/21145190.

27. Liu Y, Chen Z, Wang J. Systematic evaluation of biocompatibility of magnetic Fe3O4 nanoparticles with six different mammalian cell lines. *Journal of Nanoparticle Research*. 2010;13(1):199-212. Available at: http://www.springerlink.com/index/10.1007/s11051-010-0019-y.

28. Hsieh S, Huang BY, Hsieh SL, et al. Green fabrication of agar-conjugated Fe3O4 magnetic nanoparticles. *Nanotechnology*. 2010;21(44):445601. Available at: http://www.ncbi.nlm.nih.gov/pubmed/20935349

29. Owens GK. Regulation of differentiation of vascular smooth muscle cells. *Physiological reviews*. 1995;75(3):487-517. Available at: http://www.ncbi.nlm.nih.gov/pubmed/11443134

30. Mofrad, Mohammed R.K. "Rheology of the Cytoskeleton." *Annual Review of Fluid Mechanics*, 2009, 43: 433-453.

31. Worth NF, Rolfe BE, Song J, Campbell GR. Vascular smooth muscle cell phenotypic modulation in culture is associated with reorganisation of contractile and cytoskeletal proteins. *Cell motility and the cytoskeleton*. 2001;49(3):130-45. Available at: http://www.ncbi.nlm.nih.gov/pubmed/11668582

32. Brien ERO, Alpers CE, Stewart DK, et al. Expedited Publication Proliferation in Primary and Restenotic Coronary Atherectomy Tissue Implications for Antiproliferative Therapy. *Circulation Research*.223-231.

33. Wilcox JN. Analysis of local gene expression in human atherosclerotic plaques. J Vasc Surg 992;15:913-6.

34. Orlandi A, Ropraz P, Gabbiani G. Proliferative activity and alphasmooth muscle actin expression in cultured rat aortic smooth muscle cells are differently modulated by transforming growth factor-beta 1 and heparin. Exp Cell Res 1994;214:528-36.

35. Shier D, Butler J, Lewis R. Holes Human Anatomy & Physiology. 2007;589.

36. Shah PK, Falk E, Badimon JJ, Fernandez-Ortiz A, Mailhac A, Villareal- Levy G, et al. Human monocyte-derived macrophages induce collagen breakdown in fibrous caps of atherosclerotic plaques. Potential role of matrix-degrading metalloproteinases and implications for plaque rupture. Circulation 1995;92:1565-9.

37. Hemmer JD, Dean D, Vertegel a, Langan III E, LaBerge M. Effects of serum deprivation on the mechanical properties of adherent vascular smooth muscle cells. *Proceedings of the Institution of Mechanical Engineers, Part H: Journal of Engineering in Medicine*. 2008;222(5):761-772. Available at:

http://journals.pepublishing.com/openurl.asp?genre=article&id=doi:10.1243/09544119JEIM371.